MASSACHUSETTS INSTITUTE OF TECHNOLOGY

LINCOLN LABORATORY

MORPHOLOGY OF IONOSPHERIC SCINTILLATION

R. K. CRANE

Group 61

TECHNICAL NOTE 1974-29

21 MAY 1974

LEXINGTON MASSACHUSETTS

ABSTRACT

Available observations of scintillation from Millstone and other facilities were analyzed to evaluate the adequacy of existing models used to interpret scintillation data and to provide communications specialists with information for system design. The variation of scintillation with frequency, polarization, elevation angles, time of day, season of year and geophysical parameters such as sunspot number and magnetic activity were examined. The observations show that in the limit of weak scintillation, the scintillation index varies as $(\text{wavelength})^{1.5}$ and as the cosecant of the elevation angle. The computations based upon available long term scintillation data indicate that for zenith paths at 254 MHz, scintillation periods characterized by fades greater than 6 dB 1% of the time will occur 15% of the year in the equatorial region, 0.2% of the year in the auroral and high latitude region, and less than 0.1% of the year at mid-latitudes. For a 20° elevation angle the percentages will be 25%, 25% and less than 6%, respectively. The data further show that neither polarization nor frequency diversity will be useful for mitigating the effects of scintillation but space or time diversity may be of use.

Morphology of Ionospheric Scintillation

I. INTRODUCTION

This report is directed toward providing information to communication systems designers first about scintillation as observed in a single experiment, second about the adequacy of the existing models used to interpret scintillation data, and finally about the variation of scintillation with geophysical parameters. Scintillation due to electron density fluctuations has been observed on line-of-sight paths through the ionosphere at frequencies ranging from 20 MHz to 6 GHz. Frequencies between 100 and 400 MHz are emphasized in this paper because of their immediate concern in system design. An exhaustive literature exists on the subject of ionospheric scintillation. The references cited in this paper are not complete and are only intended to be illustrative. When possible the references will be to measurements made at frequencies in the 100- to 400-MHz range.

Early radioastronomical observations of sources of small angular extent exhibited significant intensity fluctuations. Spaced receiver measurements made at the Jodrell Bank Experiment Station[1] at 81.5 MHz showed that the intensity fluctuations originated in the F-region of the ionosphere, were correlated with the occurrence of spread-F, and formed a random intensity pattern on the ground with a correlation distance of approximately 4 km.

Current knowledge of received signal fluctuations or scintillation caused by the ionosphere has been derived from a large number of observations of amplitude fluctuations made at meter, decimeter and centimeter wavelengths. The observations have been made over the past two decades at a number of locations using radio stars or satellite-borne sources. The data have generally been recorded on strip charts. Various scintillation indices have been used to characterize the appearance of the recorded data on the charts. The scintillation indices were often subjectively estimated or, in recent years, calculated using the extreme values observed on short sections of the recording.[2] Information about the dependence of scintillation on geophysical parameters such as invariant latitude, magnetic activity index, and sunspot number has been published from summaries of the behavior of the qualitative scintillation index values compiled from available experimental data.[3-8]

Prediction of fading statistics for the design of communication systems requires more than a cataloging of data from available observations. Most of the experimental data are from observations of limited duration for path geometries, frequencies, and locations different from the system to be designed. To obtain fading statistics for system design, either additional experiments must be made using precisely the frequency and path geometry of the proposed system or one of the diffraction or scintillation

models must be used to interpret available data. The recent discovery of scintillation at 4 and 6 GHz in the equatorial region[9,10] was a surprise because it was not predicted by the then current model.

Booker et al.[11] proposed that diffraction by fluctuations of electron density in the ionosphere could cause the observed scintillation and that the effect of the electron density fluctuations could be modeled by a thin phase changing diffraction screen. Currently, scintillation phenomena are usually modeled as being caused by a thin screen using the refinements to the original analysis made by Mercier[12] and Briggs and Parkin.[13] The refinements included the introduction of a Gaussian spatial correlation function to describe the anisotropic fluctuations in electron density at and above the screen. Measurements of the spatial and temporal correlation properties of the fluctuations observed at the ground are often characterized by the scale size or correlation distance for the ionospheric diffraction screen using the Gaussian correlation function assumption.[14,15]

Recent observations have shown that the region of the ionosphere causing the fluctuations is often quite thick[16] and the thin screen model may not be adequate. The effects of random fluctuations of refractive index (or electron content) in a thick region may be analyzed using the Born (single scattering) approximation to the wave equation[17] or the Rytov method (method of smooth perturbations)[18] when the scintillation index is not too large. In

the limit of weak scintillation, all three approximate methods are identical. For strong scintillation, multiple scattering must be taken into account and none of the models is adequate.

II. MILLSTONE OBSERVATIONS

Experiment Description

Observations of scintillation at 150 and 400 MHz were made during the period January 1971 to March 1973 using U.S. Navy Navigation System satellites and receivers at the Millstone Hill Radar Facility.[19] The satellites transmitted phase coherent signals which were simultaneously recorded at the receiver site. The UHF (400 MHz) receiver system included the 84-foot Millstone Hill antenna equipped for elevation and azimuth tracking and simultaneous observations using right- and left-hand circular polarization; a phase lock tracking receiver; and analog to digital conversion of the principal polarization channel AGC voltage, error channel signals, and the in-phase and quadrature orthogonal polarization channel voltages (referenced to the principal polarization signal). The data were sampled at 15 times per second together with time, antenna pointing angle, and the VHF data and recorded on digital magnetic tape for post measurement analysis. The VHF receiver system provided in-phase and quadrature voltages for the 150-MHz signal referenced to the phase of the UHF signal divided down by the ratio of the frequencies. The VHF antenna was an eleven-element yagi

mounted on one of the feed struts of the Millstone antenna.

The satellites were in circumpolar orbit at an approximate altitude of 1000 km and were tracked from horizon-to-horizon. For each pass the average signal levels at each frequency varied by about 10 dB. The VHF receiver system had a predetection bandwidth of approximately 250 Hz. The UHF prediction bandwidth was approximately 10 kHz and the AGC system had an effective bandwidth (closed loop) of 250 Hz. The signal-to-noise ratio for optimum observing conditions was approximately 35 dB at UHF and 25 dB at VHF. The receiver system was calibrated prior to each satellite pass.

Amplitude Fluctuations

Sample observations of received signal level at both frequencies are shown in Fig. 1. The data are for a pass during the most severe magnetic disturbance that occurred during the experiment (the planetary three-hour magnetic activity index, Kp, equalled 8^+ at the time of the pass). The quiet conditions were observed to the south, the disturbed conditions through the auroral region to the north. Each 1/15-sec sample is displayed. The data for quiet conditions show fluctuations at VHF due to surface reflection multipath and weak scintillation and fluctuations at UHF due to weak scintillation. Faraday fading of the linearly polarized VHF signal is also evident as noted in the figure. Under disturbed conditions, peak-to-peak level changes

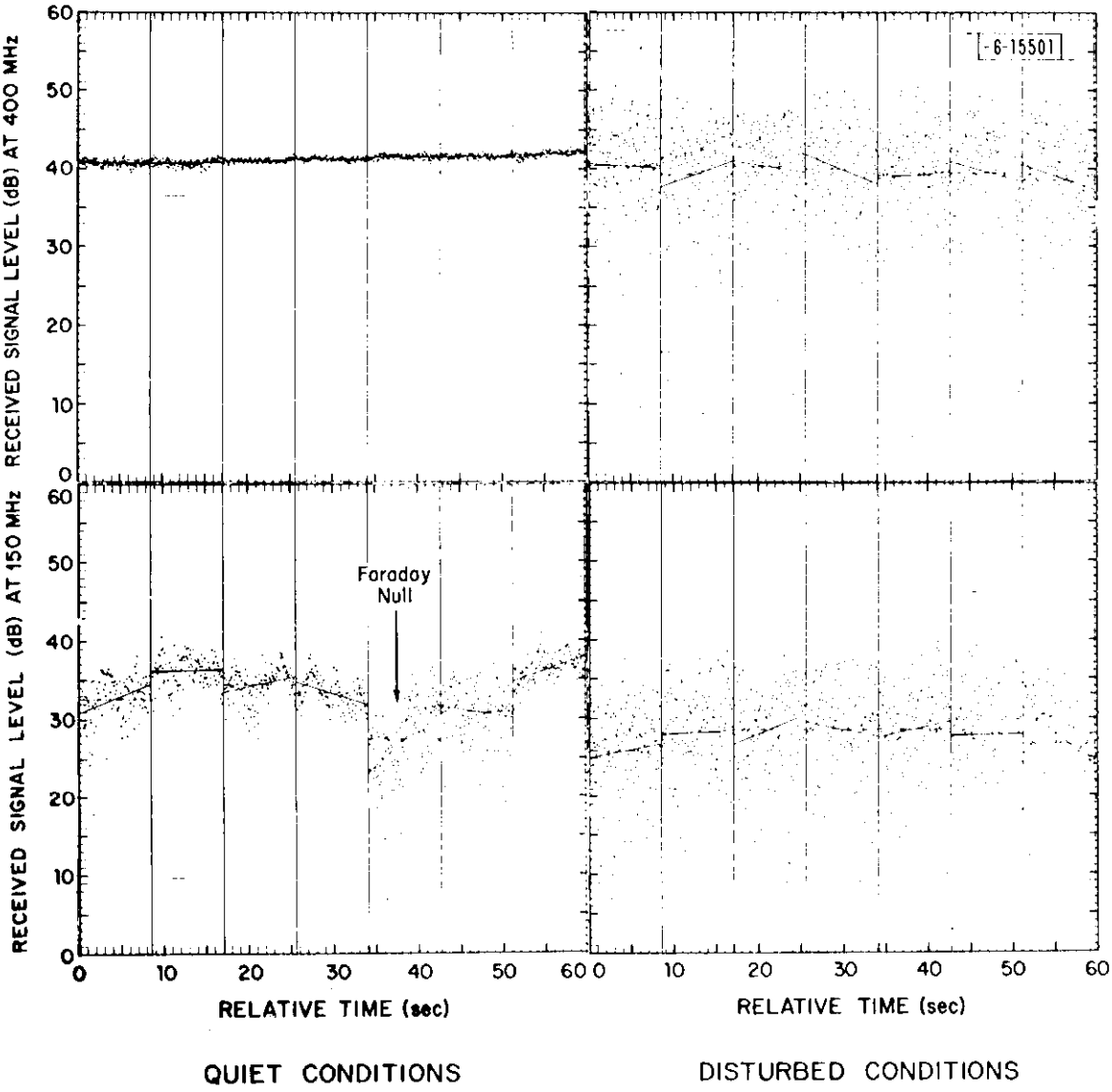

Fig. 1 UHF and VHF amplitude measurements obtained from a pass of Object #3133 on 4 August 1972.

of 45 dB at 400 MHz and 40 dB at 150 MHz are evident.

The data displayed in Fig. 1 are for roughly the same elevation angles, the mid-point elevation angle for the one-minute quiet period was 7.6°; the mid-point elevation for the disturbed period was 8.1°. For lines-of-sight to the satellite at these elevation angles, the undisturbed signal levels should be identical for observations to the north and to the south of the receiver site. The detailed Faraday null structure of the 150-MHz signal will change, however, due to differences in the mean properties of the ionosphere. The sampled data were analyzed in overlapping 8.5-second intervals. The mean and linear least square fit lines for the logarithm of the signal amplitude are displayed between the vertical lines for alternate analysis intervals. The short analysis intervals were chosen to best provide straight-line fits to the variation in signal levels caused by the satellite, receiver geometry and Faraday fading at 150 MHz. The rms variation of the observed values about the least square lines were computed to characterize the intensity of the fluctuations. For each analysis interval and frequency, the rms variation of received power about a least square straight line fit to the observed power values was also calculated. The latter rms value, when normalized by the mean value of received power for the analysis interval is the S_4 index proposed by Briggs and Parkin.[13]

The values of S_4 for each analysis interval (with midpoints spaced by

4.3 sec) are displayed in Fig. 2 for the same satellite pass as for Fig. 1. The satellite rose in the south and the relatively quiet conditions are evident for the first five minutes of the pass. Data for elevation angles below 2° are contaminated by tropospheric scintillation and surface multipath and are not displayed. The analysis of Briggs and Parkin indicates that $S_4 = 1$ is a limiting value for strong scintillations although values as high as 1.5 are possible for the right combination of scale size and distance from the thin screen. Although strong scintillation requires a consideration of multiple scattering, no analytical multiple scattering model is available. Experimental data both for ionospheric scintillation and tropospheric scintillation at optical frequencies[20] show that for strong scintillation or multiple scattering a limiting value is reached.

An obvious limiting value is shown in Fig. 3. This figure is a plot of the rms variation of the logarithm of the received signal, σ_χ, vs time for the same pass. In Fig. 3, the 95% confidence limits for the estimated error in calculating σ_χ are also depicted. The confidence limits are based upon the number of times different electron density irregularities are observed within the first Fresnel zone due to satellite motion. The data show that σ_χ reaches a limiting value of approximately 5.6 dB at each frequency. The limiting values depicted in Figs. 2 and 3 are calculated values for a Rayleigh received signal amplitude distribution. The spread of S_4

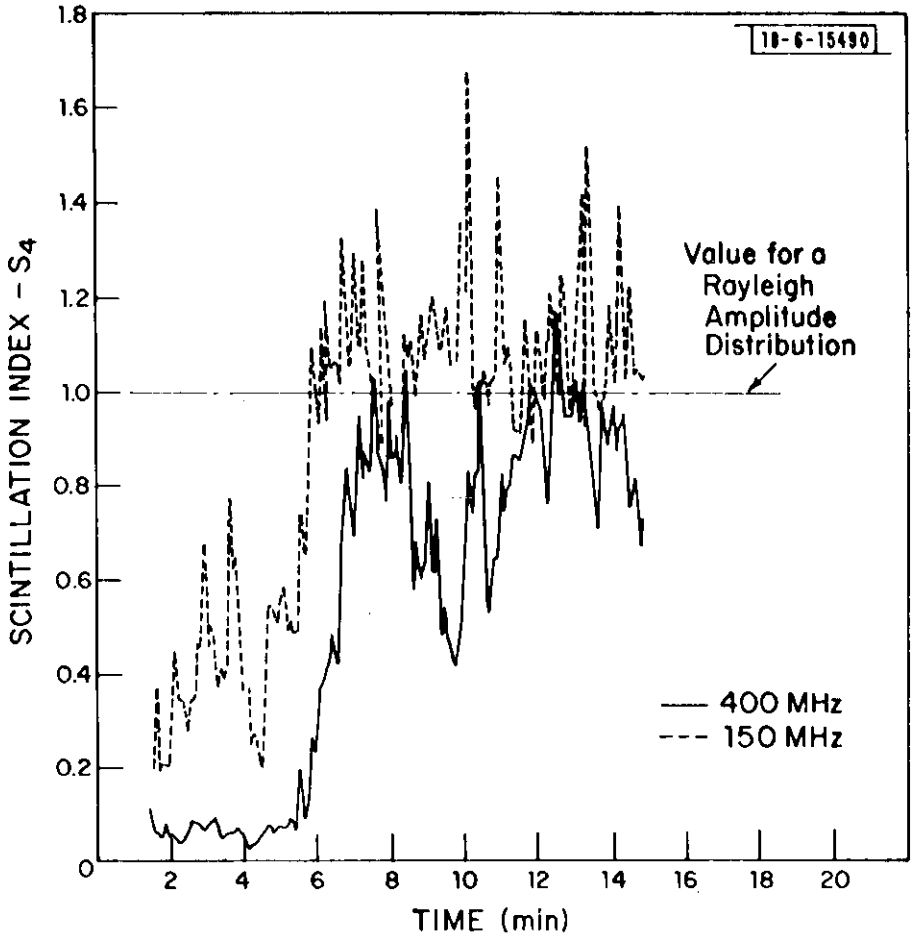

Fig. 2 S_4 vs time for pass of Object #3133 rising at 0411 GMT on 4 August 1972 (Kp = 8^+).

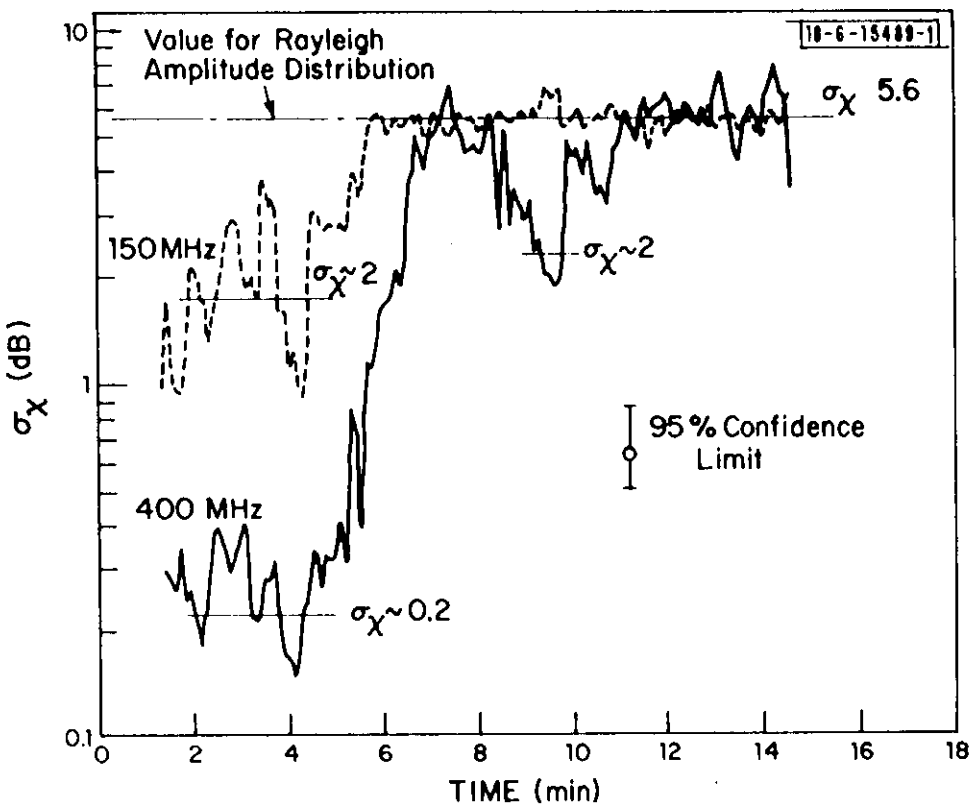

Fig. 3 σ_χ vs time for pass of Object #3133 rising at 0411 GMT on 4 August 1972 (Kp = 8^+).

values about the limiting value of 1 at 150 MHz in Fig. 2 may be due either to sampling error or to a different signal amplitude distribution.

The empirical signal amplitude distributions for the two minutes depicted in Fig. 1 are shown in Fig. 4. The data show nearly identical distributions for the two frequencies and disturbed conditions. The UHF empirical distribution function appears to be log-normal for quiet conditions. Tropospheric scintillation at optical frequencies also appears to have a log-normal distribution in the limit of strong scintillation.[21] The distribution functions are, however, definitely not log-normal for ionospheric scintillation under disturbed conditions. Bischoff and Chytil[22] proposed the use of the Nakagami-m distribution as an approximation to the empirical distributions with $m = 1/S_4^2$. Although the Nakagami-m distribution is not theoretically correct for the thin screen diffraction problem,[23] it may provide a reasonable approximate distribution and has been used for the construction of long term amplitude distribution functions.[24] The Nakagami-m distribution reduces to the Rayleigh distribution for $S_4 = 1$ and approaches the log-normal distribution for σ_χ less than 1 dB.[25] The empirical distribution functions depicted in Fig. 4 were tested against both the log- normal and Nakagami-m distributions for the calculated σ_χ values. Using the Pearson χ^2 distribution test and a 0.05 significance level, the distributions depicted in Fig. 4 were neither log-normal nor Nakagami-m. The VHF distribution

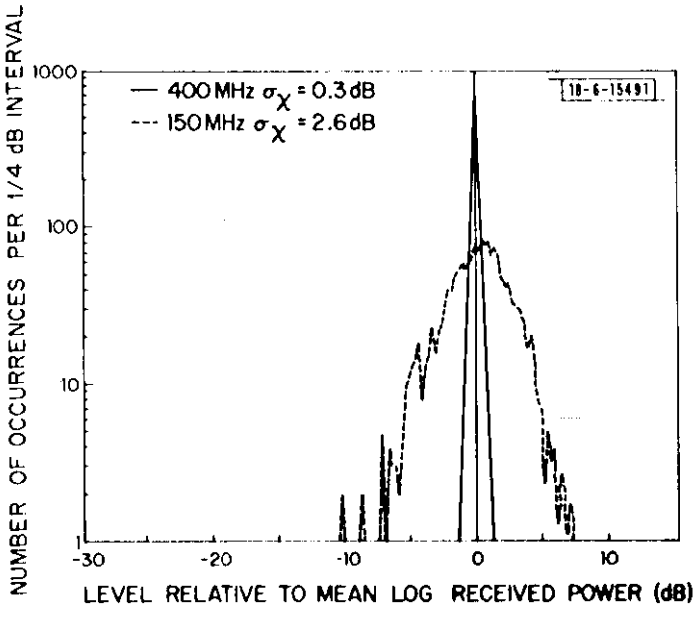

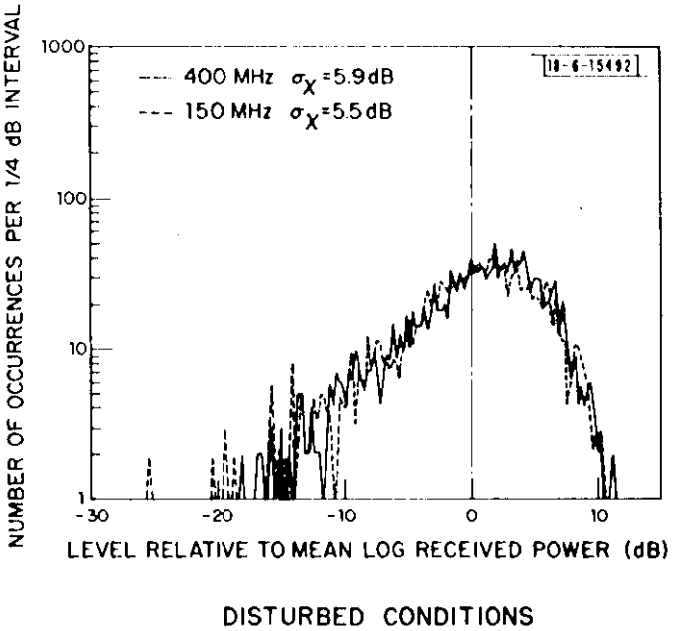

Fig. 4 Empirical amplitude distribution functions for data shown in Fig. 1.

for disturbed conditions had an m-parameter of 1.0 and tested to be Nakagami-m (Rayleigh) at a 0.01 significance level. The VHF distribution function for the minute preceding the disturbed minute (between 11 and 12 in Fig. 3) also tested to be Rayleigh with a 0.05 significance level. The UHF distribution for disturbed conditions had an m-value of 0.92 and tested to be different from a Nakagami-M distribution at reasonable significance levels. It was also observed that the in-phase and quadrature signals were correlated when m was not equal to one and were uncorrelated when m = 1.0.

The Nakagami-m distribution, although not identical to the observed distributions, does provide a useful approximation for relating the various forms of scintillation index used in the reduction of experimental data. Calculated values of S_4 and σ_χ for the satellite pass depicted in Figs. 2 and 3 are shown in Fig. 5. The relationship between S_4 and σ_χ calculated using both the Nakagami-m and log-normal distributions together with a weak scatter approximation are also shown. Of the distribution functions used, the Nakagami-m provides the better estimate of the S_4 - σ_χ relationship for the entire range of observed values. The usefulness of the Nakagami-m distribution for approximately relating the various signal variance values proposed by Briggs and Parkin and for relating the extreme value indices to other measures of scintillation is documented by Bischoff and Chytil and Whitney et al.[24]

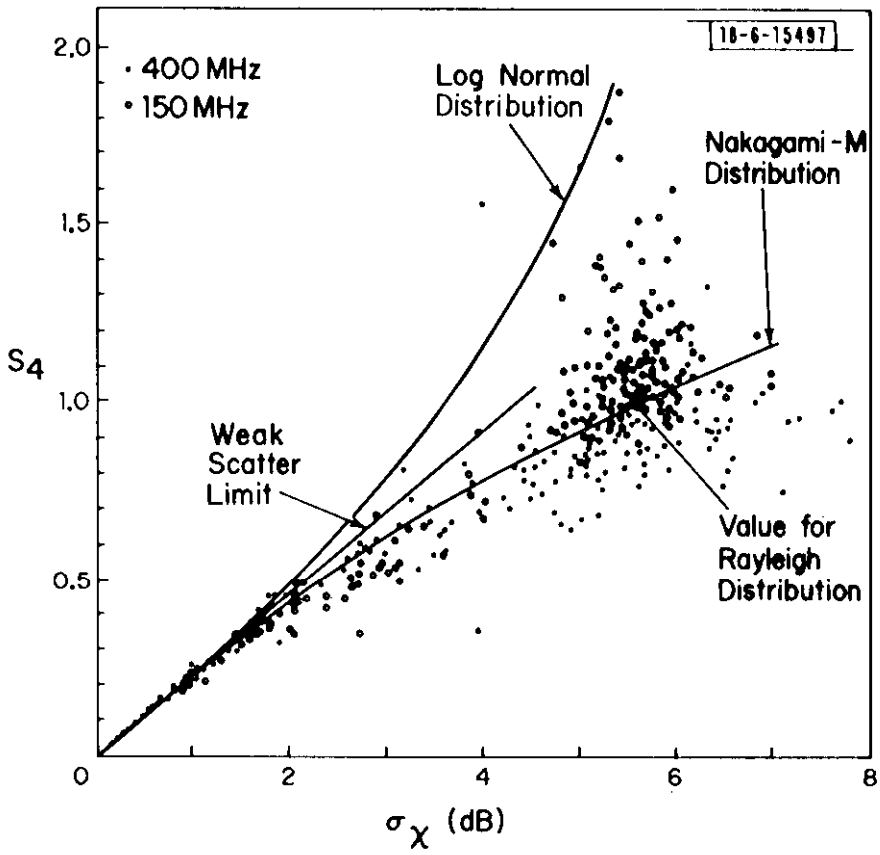

Fig. 5 S_4 vs σ_χ for pass of Object #3133 rising at 0411 GMT on 4 August 1972 ($Kp = 8^+$).

The VHF amplitude fluctuations depicted in Fig. 1 appear to be more rapid for disturbed than for quiet conditions. The temporal behavior of scintillation can be quantitatively depicted by computing distributions of the time durations the signal is below or above present thresholds. Empirical distribution functions of duration below and above a level 3 dB below the mean log received power for the disturbed conditions shown in Fig. 1 are presented in Fig. 6. The data show that the duration distribution functions are approximately exponential with different slopes for times above and below the -3 dB-threshold. The average fade duration is given by the value of time duration required to reduce the number of observations by 1/e. For the -3 dB-threshold and disturbed conditions, the average fade duration was 0.08 sec at 400 MHz and 0.05 sec at 150 MHz. The fade rate is the reciprocal of the average fade duration for a 0-dB threshold. For the quiet conditions depicted in Fig. 1, the fade rate was 3.8 Hz at UHF. For disturbed conditions, the fade rate was higher being 7.2 Hz at UHF.

The temporal behavior of scintillation may also be characterized by empirical correlation functions or power spectra. Power spectra for selected time periods from the pass depicted in Fig. 3 are displayed in Figs. 7 and 8. The power spectra were calculated using detrended log received power data from each analysis interval. The data for each interval were parabolically weighted prior to calculating the Fourier transform and the

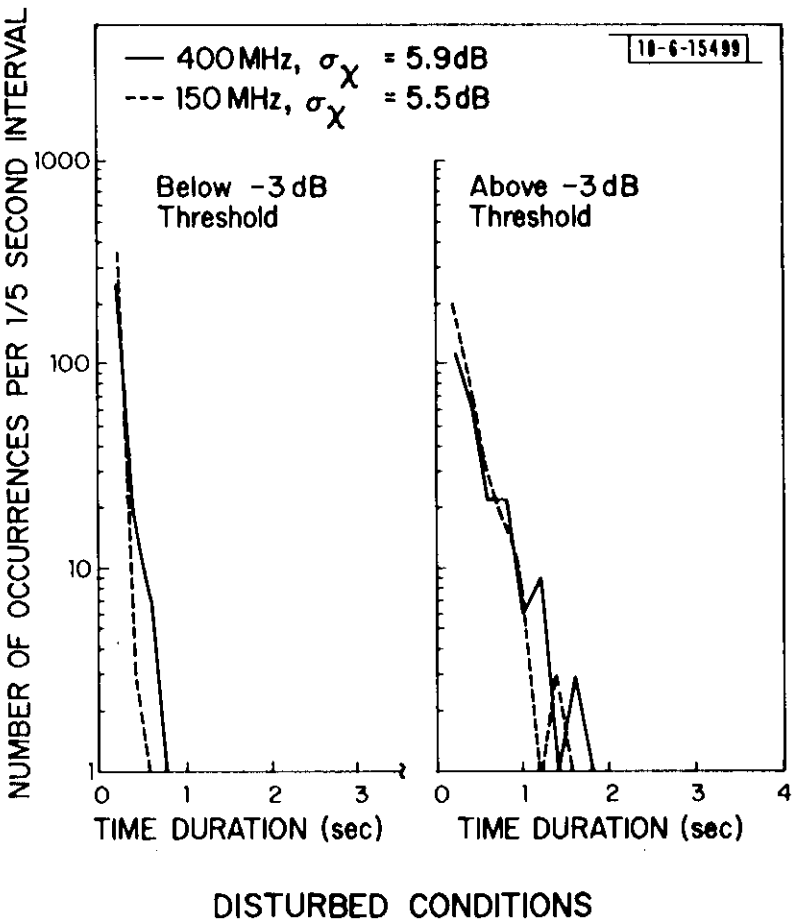

Fig. 6 Empirical distribution functions for durations below and above a -3 dB-threshold relative to the mean log received power for the data shown in Fig. 1.

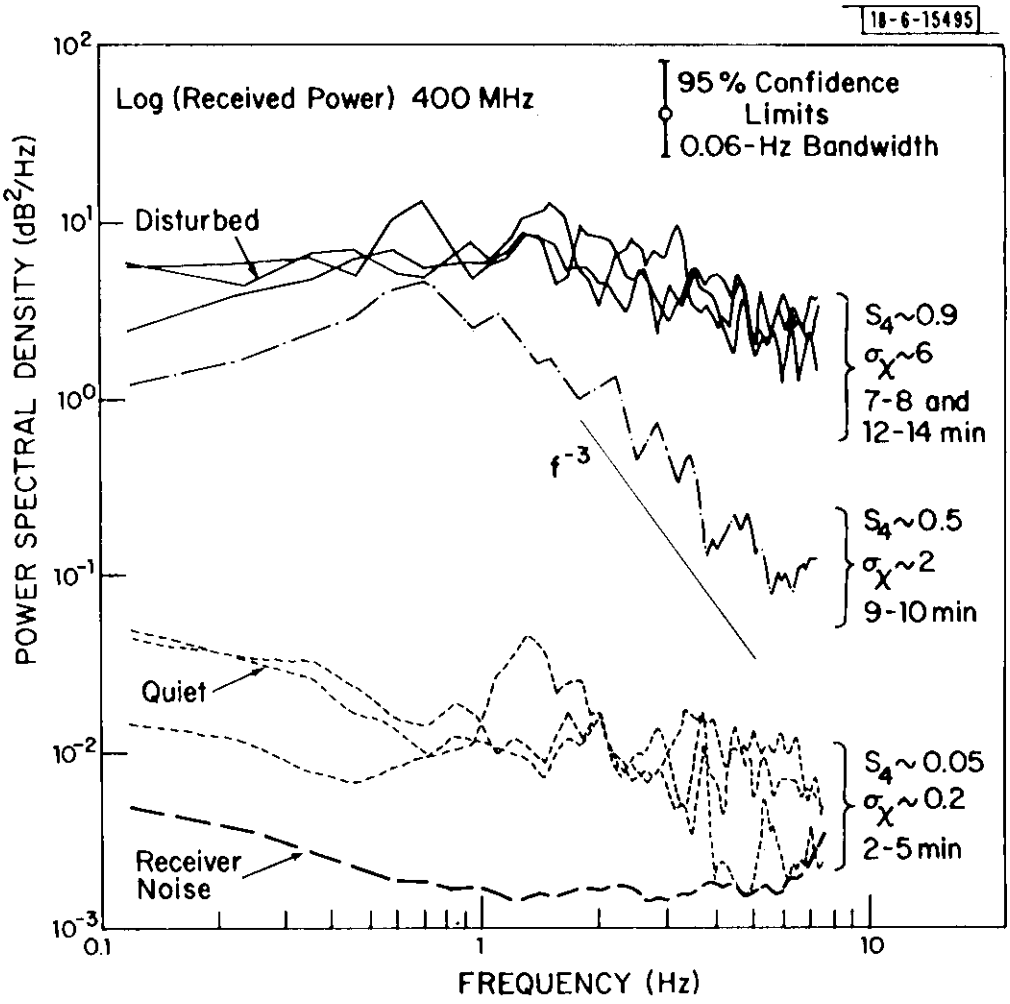

Fig. 7 UHF log amplitude power spectra for selected minutes from the pass of Object #3133 rising at 0411 GMT on 4 August 1972 (Kp = 8^+).

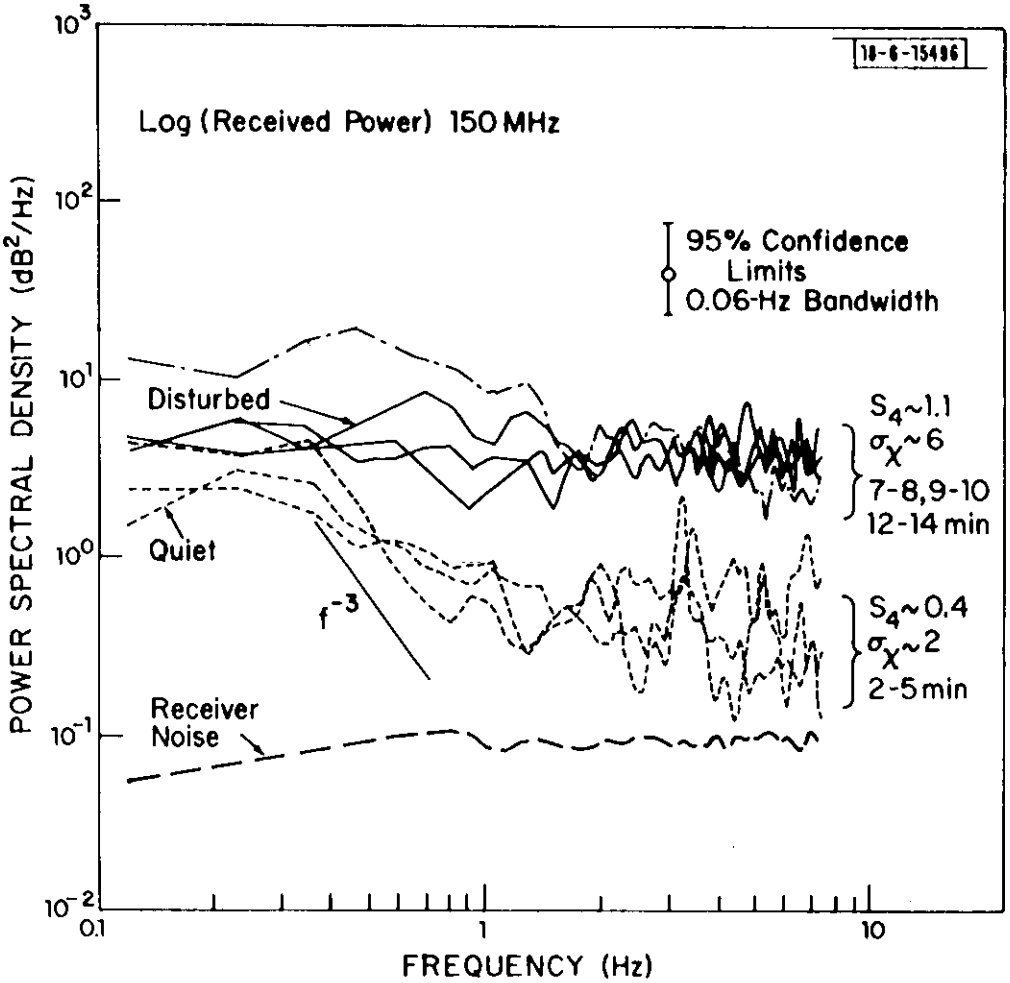

Fig. 8 VHF log amplitude power spectra for selected minutes from the pass of Object #3133 rising at 0411 GMT on 4 August 1972 (Kp = 8^+).

resultant power spectra were averaged over 13 analysis intervals within a minute. The spectra represent signal plus noise. The receiver noise levels are also depicted on each figure. The receiver bandwidths prior to sampling are approximately 250 Hz and with a sampling rate of only 15 per second (Nyquist frequency of 7.5 Hz) considerable aliasing is possible in the reported spectra. The data reported here were obtained from a satellite tracking analysis program which required the relatively slow sampling rate.

The UHF spectra for the quiet and disturbed times are identified on the figure. The dashed spectra are for minute intervals between 2 and 5 minutes as shown in Fig. 3. The horizontal lines with σ_χ values in Fig. 3 represent the duration spanned by the spectra displayed in Fig. 7. The dashed lines are for quiet or weak scintillation conditions. The quiet data are barely above receiver noise and are not useful in describing scintillation phenomena. The dot-dashed spectrum, for minute 9-10, is for a period when the strong scintillation limit was not reached. The spectra approximates a power law for frequencies greater than 1 Hz. Power law power spectra have been reported by Rufenach[26] and Singleton[27] and the power law form is evident in the data reported by Elkin and Papagiannis.[28] A line with a slope of -3 is drawn on the figure but the best fit slope for the power spectra may lie between -2 and -3. The fluctuations of the power spectra with frequency are due to the limited statistical accuracy of the

reported values. One-minute sample sizes were chosen because the process is obviously not stationary over longer time intervals (except perhaps when the strong scintillation limit is reached as shown in Fig. 3) and may well not be stationary even over a minute. Shorter sample lengths were not chosen because the statistical error would become significantly larger.

The spectra for disturbed or strong scintillation limit fluctuations are represented by solid lines. These data show little change of level with frequency implying that severe aliasing is present in the data and the sampling rate was not high enough to adequately represent the strong scattering case. The data were obtained as a part of a general propagation study and higher sampling rates would have compromised other elements of the program. The sampling rate was high enough to adequately analyze weak scintillation ($\sigma_\chi \sim 2$ on Fig. 7). What is evident in the strong scintillation data is relatively little change in the low frequency variance energy and significant increases at higher frequencies. The correlation time therefore decreases and the spectrum spreads (fade rate increases) as the strong scintillation limit is reached.

The VHF spectra for the disturbed period are also flat spectra. For quiet conditions, the σ_χ value is approximately the same as for the dot-dashed curve in Fig. 7. As in Fig. 7, the spectra at lower frequencies have almost the same levels as for the strong scintillation limit. For quiet

conditions and frequencies above 1 Hz, the signal variance to noise variance ratios for the reported spectra are not large enough to provide an adequate measure of the shape of each spectrum.

Phase Fluctuations

The phase of the signals from the satellite fluctuates when scintillation occurs. The differential phase path length was measured using the VHF in-phase and quadrature voltage values. The phase reference for the VHF signal was the phase of the UHF signal divided down by the ratio of the two frequencies. The differential phase path length values, reported in terms of phase change at 150 MHz reference the initially reported phase value, are shown in Fig. 9. The differential phase value at a sample instant is computed from the reported in-phase and quadrature voltage values and can only be determined modulo 2π. In processing the data, the assumption is made that the phase cannot change by more than π radians between successive samples. This assumption is adequate only if the data are sampled at a sufficiently high rate. The in-phase and quadrature channel bandwidths were 250 Hz prior to sampling and it is possible that phase shifts greater than 2π can occur between sampling times.

The rms variation in differential doppler and phase are depicted in Fig. 10 for the entire pass. The differential doppler values appear to show a strong scintillation limit at 4.3 Hz corresponding to the $\pi/\sqrt{3}$ rms value

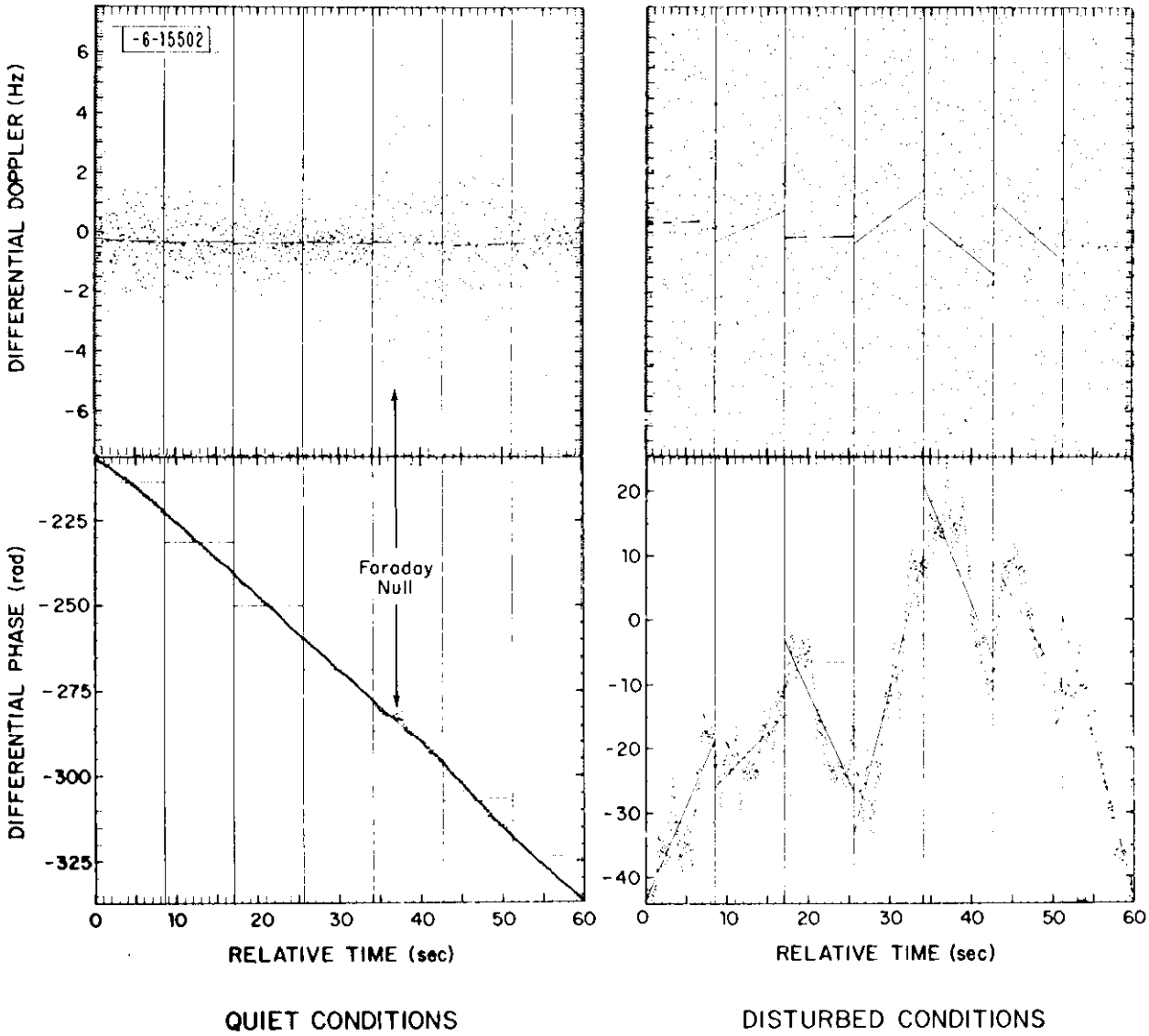

Fig. 9 Differential phase and differential doppler measurements obtained from a pass of Object #3133 rising at 0411 GMT on 4 Aug. 1972 (Kp = 8^{+}).

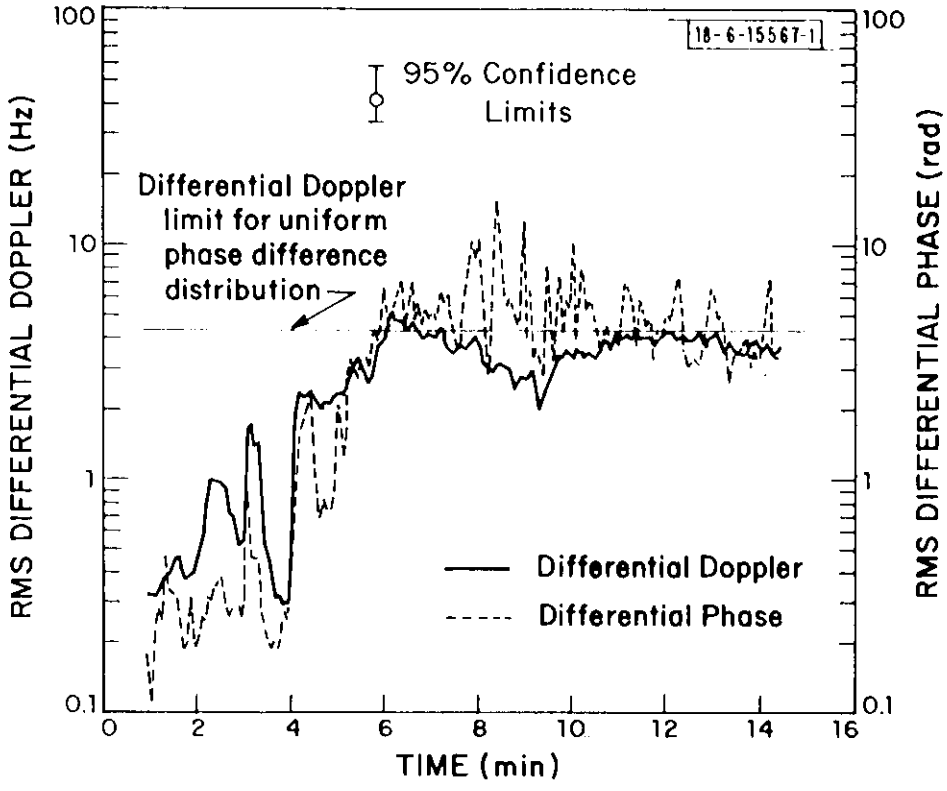

Fig. 10 RMS variations in differential phase and differential doppler for pass of Object #3133 rising at 0411 GMT on 4 August 1972 (Kp = 8^{+}).

for phase change between successive observations of a Rayleigh process. The rms variations in differential phase show more uncertainty for strong scintillation due to possible phase ambiguities.

Power spectra for the differential phase fluctuation observations are shown in Fig. 11. The dashed curves correspond to weak scintillation and a sampling rate adequate to unambiguously measure differential phase. These power spectra show a region of generally linear (power law) decrease until the data are contaminated by receiver noise. For frequencies below .3 Hz the spectra are increasing with decreasing frequency though at a lower rate than for frequencies from .3 - .6 Hz. The data at the low frequencies are, however, contaminated by the curve fitting, detrending procedure used to prepare the data for transform analysis. Phase difference power spectra observations reported by Porcello and Hughes[30] show reasonably convincing power law power spectra over a range from .1 to 10 Hz for satellites in orbits similar to those used for the Millstone measurements. The slopes of the power spectra observed by Porcello and Hughes ranged from -2.8 to -3.0. The strong scintillation data also show an f^{-2} power law behavior caused by random 2π phase jumps or ambiguities.

Depolarization

Simultaneous observations were made on both left- and right-hand circular polarizations at UHF. The transmissions were nominally right-

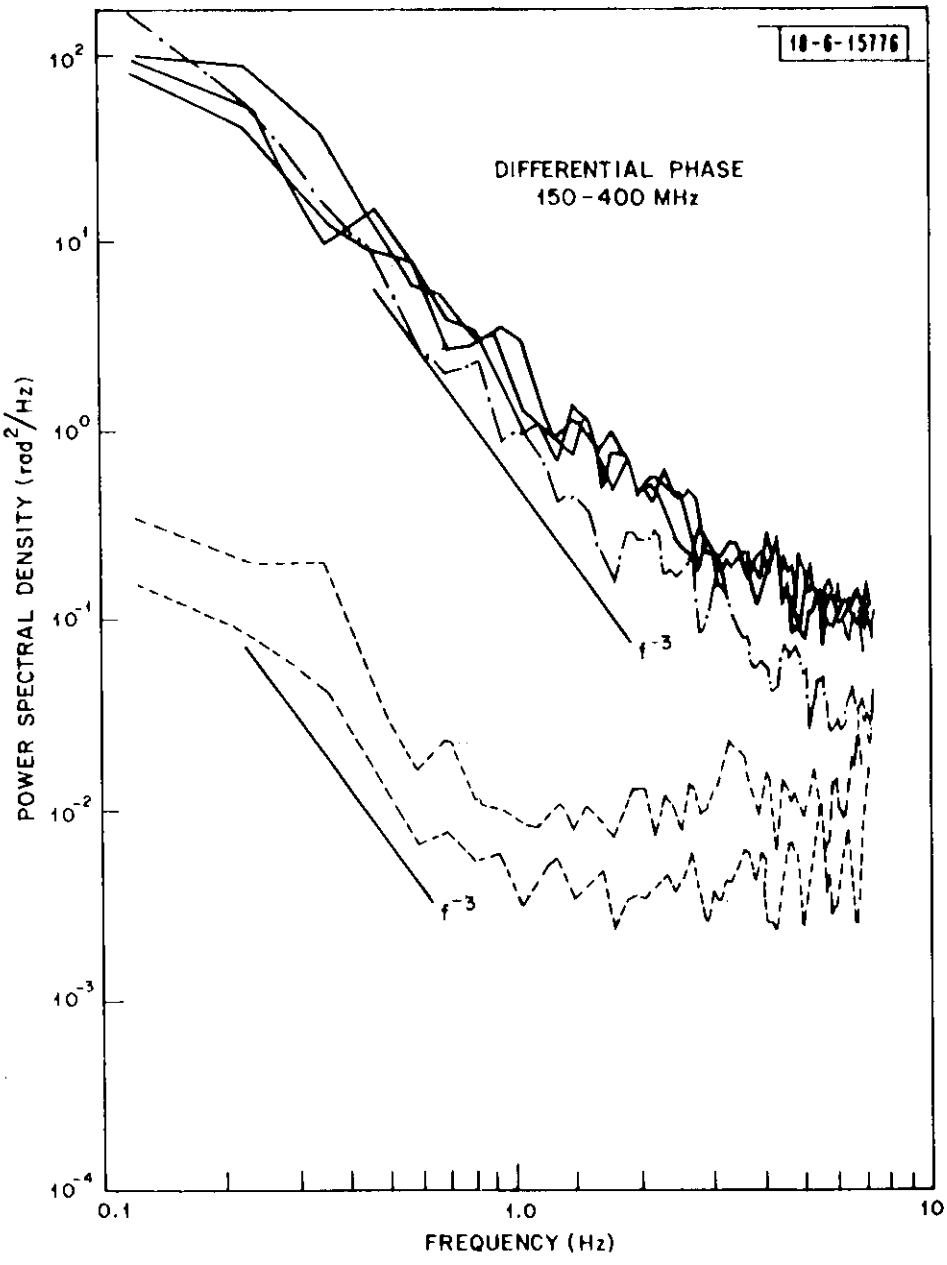

Fig. 11 Differential phase power spectra for selected minutes from the pass of Object #3133 rising at 0411 GMT on 4 August 1972 (Kp = 8^+).

hand circular but in practice were elliptically polarized. The polarization state changed slowly with changes in satellite, receiver station geometry. The orthogonal polarization receiver channel was gain controlled by the primary polarization AGC signal. The AGC control system was effective in removing fluctuations of limited dynamic range that occurred simultaneously on both channels at frequencies up to 250 Hz. For strong fluctuations with peak-to-peak spreads of more than 20 dB, the AGC system did not remove all of the simultaneous fluctuations from the orthogonal channel output and the residual fluctuations were detected. For weak scintillation, only fluctuations on the orthogonal channel that were not correlated with the principal polarization fluctuations would be detected. The signal-to-noise ratio for uncorrelated fluctuations was in excess of 20 dB for typical satellite, receiver geometries.

The rms variation of the log of the orthogonal channel amplitude and the correlation coefficient between the log of the orthogonal channel output and the log of the principal channel output is shown in Fig. 12 for the entire pass (see Fig. 3 for principal polarization variation). For weak scintillation, the output is near receiver noise and no correlation is evident. After seven minutes, the scintillation is much stronger and a low level variance is evident in the orthogonal channel data. This residual output is however correlated with the scintillation in the principal polarization channel

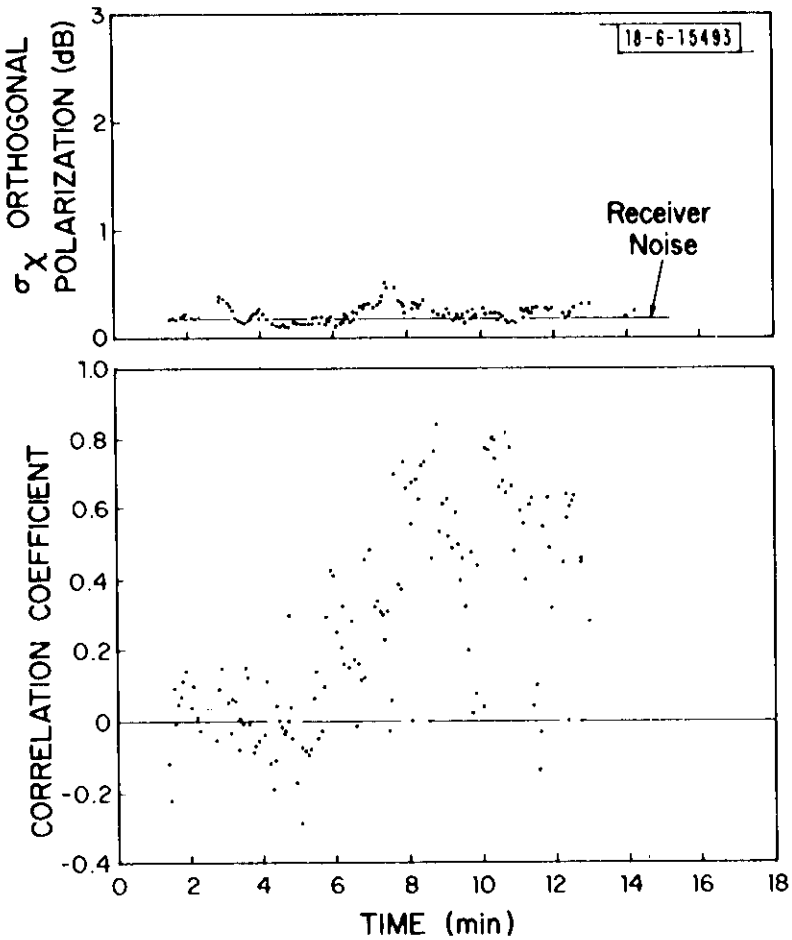

Fig. 12 Rms variation in the output from the orthogonally polarized channel and correlation coefficients between the principal and orthogonal channel outputs for pass of Object #3133 rising at 0411 GMT on 4 August 1972 (Kp = 8^{+}).

as shown in Fig. 12. The data therefore show no uncorrelated fluctuations.

These observations show that the fluctuations on both polarizations are correlated and polarization diversity systems will not be useful in combating ionospheric scintillation at UHF. If significant uncorrelated orthogonal polarization fluctuations were present they would have σ_χ values near those depicted in Fig. 3. The orthogonal channel values were significantly smaller even for the strongest scintillation levels. Similar conclusions have been drawn by Whitney and Ring[31] from limited observations made at 137 MHz for scintillation levels below the strong scintillation limit and by Koster[32] for a single set of strong scintillation observations at 137 MHz made in the equatorial region. Blank and Golden[33] reported equatorial region polarization observations at 136 and 400 MHz obtained from the low orbiting OAO-2 satellite. Their data show correlations between vertical and horizontal polarizations that range from 0.0 to 1.0 with mean values of 0.3 at 136 MHz and 0.8 at 400 MHz. It is believed that their data were seriously contaminated by surface reflection multipath (as are the 150-MHz data from Millstone) and that their results do not describe the effects of ionospheric scintillation.

Observations at frequencies lower than 54 MHz show that orthogonal circular polarization channels may fade independently[34] and diversity is possible. At frequencies below about 50 MHz, the ordinary and extraordinary

rays may be separated by more than the radius of the first Fresnel zone and the electron density fluctuations causing scintillation will not be correlated for two orthogonal polarizations.[35] Sufficient separation between ordinary and extraordinary ray paths for the fluctuations to become independent is not possible at frequencies above 100 MHz.

III. CARRIER FREQUENCY DEPENDENCE OF THE UHF, VHF OBSERVATIONS

Frequency Dependence of the Scintillation Index

The data presented above are provided to illustrate the characteristics of scintillation as observed at UHF and VHF. These data can be used to provide information about scintillation at other locations, frequencies, and path geometries only if a model is available for their interpretation. In the limit of weak scintillation, the available models discussed above all relate the power spectrum of amplitude (or log amplitude) as observed on the ground to the power spectrum of the electron density fluctuations modified by the effects of the scattering process (Fresnel filtering). The power spectrum of temporal changes observed on a line-of-sight path to a low orbiting satellite may be related to the power spectrum of spatial fluctuations of electron density by assuming that the electron density fluctuations do not change during the time the line-of-sight sweeps through a disturbed region of the ionosphere.

Early models of scintillation assumed that the spatial correlation

function for electron density fluctuations was approximately Gaussian with different scale sizes along and perpendicular to the magnetic field lines.[13] The Gaussian model implies a Gaussian power spectrum with power spectral densities decreasing rapdily for spatial frequencies above the reciprocal of the scale size. The combination of the Gaussian spectrum and Fresnel filtering also implies a decrease in power spectral density for spatial frequencies smaller than the reciprocal of the scale size. In the limit of high frequencies corresponding to spatial frequencies larger than the reciprocal of the Fresnel zone size, the spectrum observed on the ground should be identical to the two-dimensional spectrum of electron density fluctuations observed in a plane normal to the direction of the propagation path. For a Gaussian model, the high frequency limit should have a parabolic shape with increasing negative slopes for increasing frequency when observed for weak scintillation. The dot-dashed curve in Fig. 7 has sufficient signal variance to noise variance ratio to show that the shape of the spectrum for high frequencies is indicative of a power-law power spectrum rather than a Gaussian power spectrum.[26] Similar results have been obtained by Singleton.[27]

Power spectra at both UHF and VHF with a reasonably high signal variance to noise variance ratio and for weak scintillation are shown in Fig. 13. These spectra are for the same one-minute observation periods

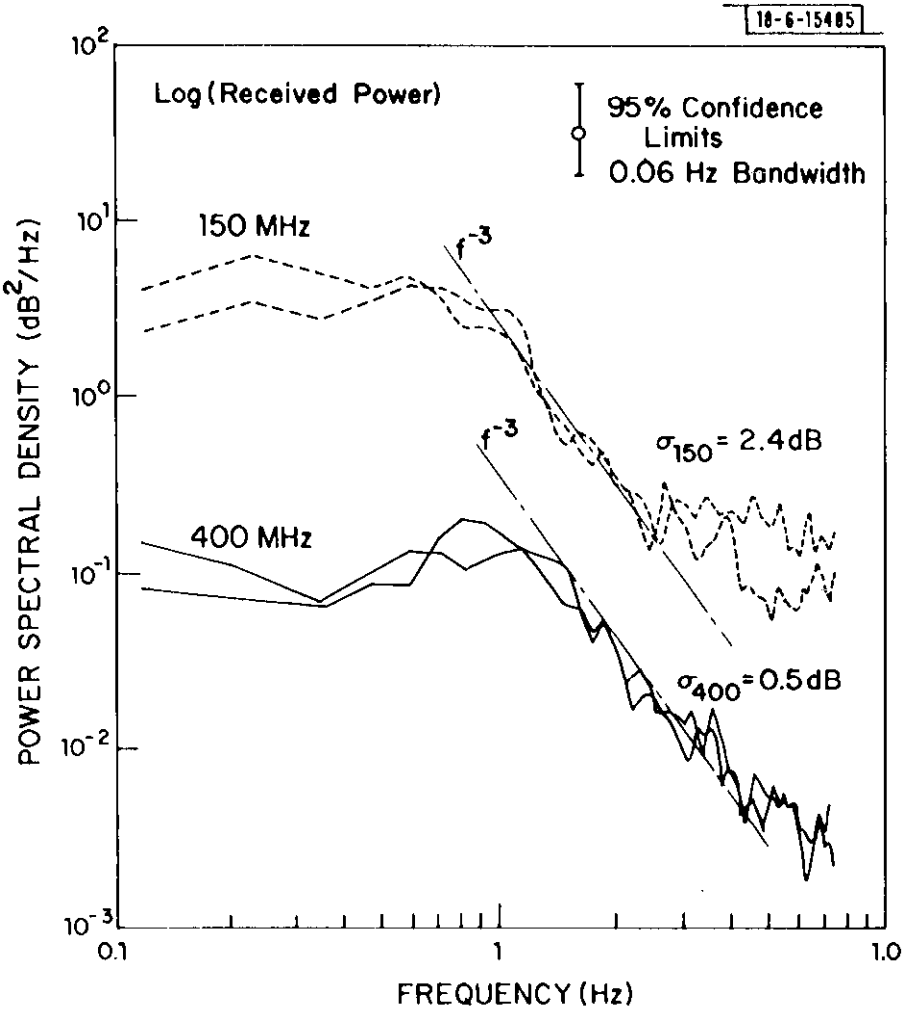

Fig. 13 Power spectra for log received power fluctuations at both UHF and VHF for the same one minute observation period of the pass of Object #3133, 5 August 1972 at 0334 GMT (Kp = 8^+).

and for a time period when the individual rms log amplitude values for each analysis interval changed little at both frequencies (the process was nearly stationary). Both spectra show power-law high frequency regions. The scintillation models predict that the power spectral density values should increase by the square of the ratio of the carrier wavelength. The best fit straight lines to both observed spectra having a wavelength squared separation are shown on the figure. The slope of these lines is approximately -3. This corresponds to a power-law dependence for the three-dimensional spatial power spectrum of electron density fluctuations with an index of 4($S \propto k^{-p}$, S = power spectral density, k = wavenumber, p = index) and a one-dimensional spectrum with an index of 2. In situ measurements made with the OGO-6 satellite also show one-dimensional power-law power spectra with indices ranging from 1.5 to 2.3 and having an average value of 1.9.[36] The data presented in Fig. 13 are for observations to the northwest at an elevation angle of 18°. For the satellite, receiver station geometry, the Fresnel zone size at a height of 300 km was 0.7 km at 400 MHz and 1.1 km at 150 MHz. The ray moved at approximately 1.0 km/sec through the ionosphere (velocity perpendicular to the line-of-sight at 300 km). The ratio of the frequencies at which each of the spectra flatten (1.5 Hz at 400 MHz to 0.9 Hz at 150 MHz) is approximately the same as the ratio of their Fresnel zone flushing frequencies (ratio of the ray velocity perpendicu-

lar to the ray direction to Fresnel zone size). Frequencies higher than the flushing frequency correspond to scale sizes smaller than the Fresnel zone size.

The weak scintillation theory for a power-law spectrum predicts a scintillation index (S_4 or σ_χ) frequency dependence given by[37]

$$\left(\frac{\sigma_{\chi_1}}{\sigma_{\chi_2}}\right) \propto \left(\frac{\lambda_1}{\lambda_2}\right)^{(p+2)/4} = \left(\frac{\lambda_1}{\lambda_2}\right)^{\eta}$$

where λ is wavelength, the subscripts refer to the carrier frequencies, and η is the spectral index. For a three-dimensional power-law index of 4, the spectral index is 1.5. Using this spectral index, σ_χ at 150 MHz should be 4.4 times σ_χ at 400 MHz. For the data displayed in Fig. 13, σ_χ at 400 MHz was 0.5 dB, σ_χ at 150 MHz was 2.4 dB, and the predicted value using $\eta = 1.5$ is 2.3 dB, well within the measurement error of the observed value. The relationship between σ_χ at 150 MHz and σ_χ at 400 MHz for a pass with reasonably high signal variance to noise variance ratios is shown on Fig. 14. The weak scintillation limit curve corresponding to a spectral index of 1.5 is shown together with the strong scintillation limit. The data appear to lie along the weak scintillation estimate curve until the strong scintillation limit is reached, then σ_χ remains at the latter value.

The frequency dependence of ionospheric scintillation has received

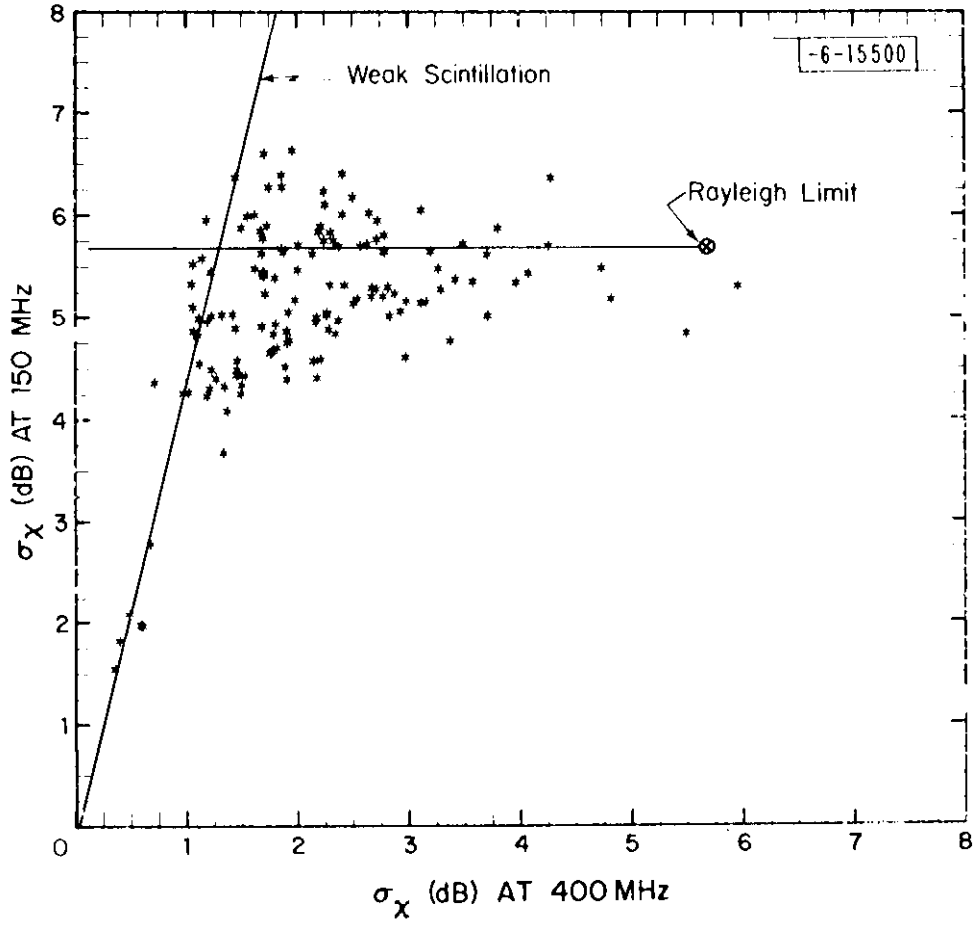

Fig. 14 RMS variation of log received power at VHF vs simultaneously observed value at UHF from pass of Object #3133 rising at 2342 GMT on 4 August 1972 (Kp = 8^+).

considerable attention in the literature. The thin phase screen, Gaussian correlation function model predicted a spectral index of two when the scale size was larger than the first Fresnel zone radius (near field limit) and of one when the scale size was smaller (far field limit).[13] The power-law power spectra model predicts a single value for weak scintillation for all cases (provided the power law holds over all scale sizes). Experimental verification of the frequency dependence prediction is difficult because the scintillation index must be less than the saturation limit value at both the high and low frequency. For strong scintillation at both frequencies, the empirically determined spectral index would be zero. For a random selection of observations, the empirical spectral index should lie between 0 and 1.5. Surface multipath, signal-to-noise, and measurement dynamic range problems inherent in many of the early measurements could further degrade the estimates of spectral index. From Fig. 3 for the period between two and five minutes the ratio of σ_χ values is approximately 10 implying a spectral index of 2.3. As shown in Fig. 8, the lower frequency was contaminated by surface multipath and receiver noise causing a fictitiously high spectral index estimate.

Simultaneous observations of radio star scintillation reported by Basu et al.[38] showed a spectral index value of approximately 1.5 for frequencies of 112 and 224 MHz and a lower value for the 63, 112 MHz frequency

pair. The lower value for the lower frequency presumably is caused by strong scintillation data. These observations were made at the Sagamore Hill Radio Observatory, less than 100 km from Millstone. Aarons[39] reported observations at frequencies between 22 and 39 MHz from Arecibo, Puerto Rico, under weak scintillation conditions and found a median spectral index of 1.6. Amplitude scintillations observed by Lawrence et al.[4] at 53 and 108 MHz show a median spectral index value of 1.5 for S_1 values below 0.01 ($\sim S_4 = 0.5$) at 53 MHz. Early observations reported by Chivers[40] made at Jodrell Bank Experimental Station at several frequencies between 36 and 408 MHz using radio stars had mean spectral indices ranging from 1.9 to 2.1. Observations also made at Jodrell Bank at 79 and 1390 MHz and reported by Chivers and Davies[41] showed, in the limit of weak scatter at 79 MHz and just detectable fluctuations at 1390 MHz, a value of η near 1.5.

Aarons et al.[42] and Allen[43] argue, for observations made above 63 MHz from the Sagamore Hill Radio Observatory, that a spectral index of 2.0 best fits their data in the limit of weak scatter although their plots of scintillation index vs η curve have a median value of 1.6 as long as the scintillation index at 113 MHz is between 5 and 25% (S_4 at 63 MHz less than 0.6 and measurable scintillation at 113 MHz). Recently reported observations from the same observatory at frequencies of 137 and 412 MHz by Whitney et al. show, for similar weak but measurable scintillation conditions,

a distribution of η values between 1.2 and 1.8 with a mean value of 1.49 $\pm$ 0.05.

Only a limited number of spectral index estimations have been made for equatorial regions. Blank and Golden[33] report $\eta \sim 0.2$ to 0.3 for frequencies between 137 and 400 MHz. They comment that the results pertain, in part, to strong scatter. Craft and Westerlund[44] reported a value $\eta \sim 2$ for equatorial measurements at 4 and 6 GHz. The latter observations were for weak scintillation and may indicate either the existence of an inner scale where the power-law region ends and a different power spectrum shape occurs or the problems of detecting small fluctuations in noise.

Correlation of Amplitude Fluctuations At Two Frequencies

The rms amplitude fluctuations decrease with increasing frequency for weak scatter. They are also correlated over a wide frequency range. Calculations of the expected correlation coefficient for power-law indices ranging from 3 to 4 are shown in Fig. 15. Similar calculations for Gaussian spectra have been made by Budden.[49] Since the available power spectra and frequency dependence data support the power-law model, the Gaussian model predictions will not be presented. Measured correlation coefficients for the Millstone data and from available papers are also presented. The $p = 4$ curve provides the best estimate based upon the above analysis and should represent the upper bound for measurements for each Δf value. The lower

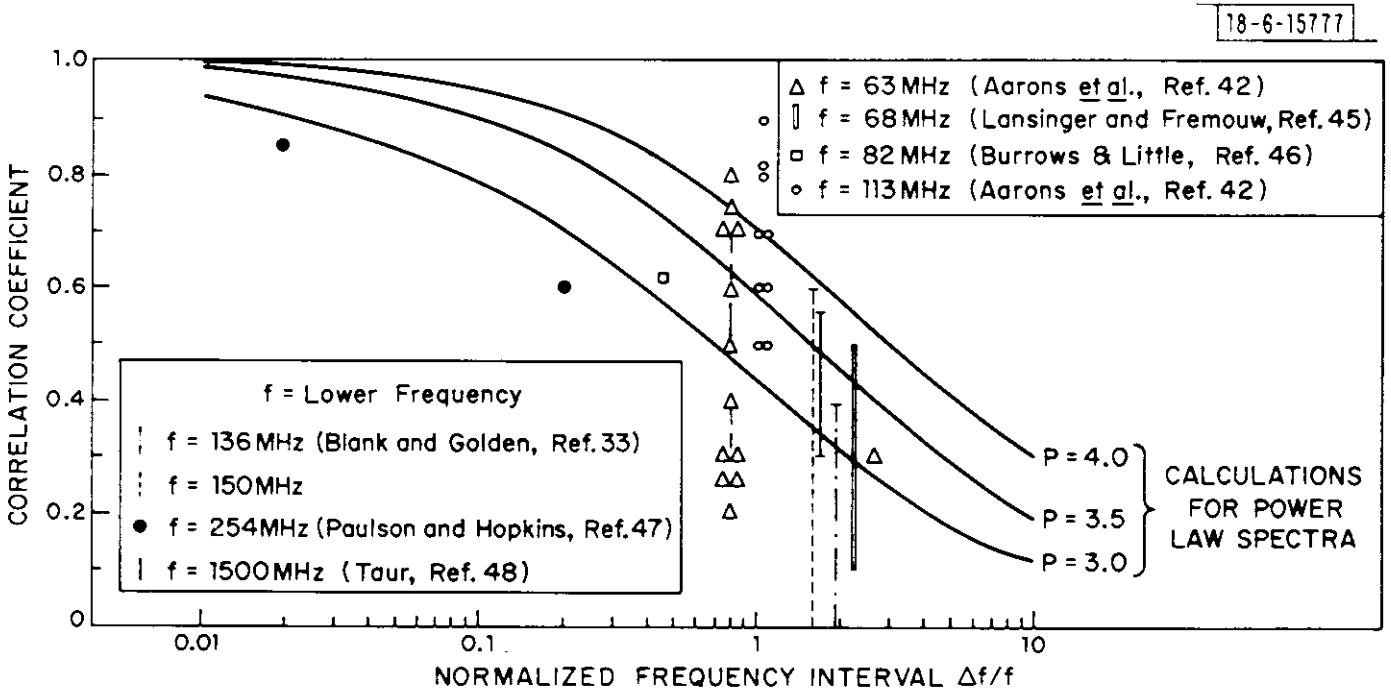

Fig. 15 Two frequency correlation functions for amplitude fluctuations.

frequencies used in the two frequency observations are listed in the figure. For strong scintillation, the correlation coefficient should be lower than the calculated values due to the effect of saturation and spectral broadening which happens first at the lower frequency. For low frequency observations, the first Fresnel zones at each frequency may not overlap due to different ionospheric refraction at each frequency. For an elevation angle of 10°, rays at 150 and 400 MHz are separated by more than 5 km at a height of 300 km. The Millstone observations depicted in Fig. 1 show no correlation between the two frequencies. Since the elevation angles are less than 10° for the data depicted in Fig. 1 and the first Fresnel zone radii are less than 1.3 km, no correlation was expected.

The data displayed on Fig. 15 show reasonable agreement with the calculations. The data reported by Taur[48] for frequencies of 1.5 and 4.0 GHz are for weak scintillation only. These data show better agreement for p between 3 and 3.5 that at 4. This again may indicate a change in the power spectrum of electron density fluctuations at small scale sizes in the equatorial region. The observations reported above for auroral and mid-latitude sites are all in reasonable agreement with a power-law power spectrum model with an index of 4 for the three-dimensional fluctuations of electron density. The situation for equatorial regions is not as convincing and more data are required. It is, however, evident that the correlation

coefficients are reasonably high over a wide frequency range. This implies that for high elevation angles where the rays at each frequency are separated by less than a Fresnel zone radius (at the higher frequency), extremely wide frequency separations (~10 to 1) are required to provide adequate frequency diversity operation and frequency diversity is not useful in combating the effects of scintillation.

IV. PROBABILITY OF OCCURRENCE OF SCINTILLATION

Morphological studies of the dependence of scintillation on geophysical parameters[3, 7, 24] have shown that scintillation is most severe and prevalent in and north of the auroral zone and near the geomagnetic equator. These regions, the auroral plus high latitude region and the equatorial region, are shown as shaded areas on the map in Fig. 16. The unshaded belts between the auroral and equatorial regions are called mid-latitude regions. Invariant latitude is frequently used in mapping scintillation. The invariant latitude Λ is derived from a magnetic field aligned coordinate system proposed by McIlwain[50] to map magnetically trapped particles. The geographical locations of invariant latitude contours at a height of 300 km are shown on Fig. 16. Observations at frequencies between 20 and 6000 MHz have generally shown that the auroral plus high latitude region exists at $|\Lambda| \geq 55°$ and the equatorial region exists at $|\Lambda| \leq 20°$. The boundaries of these regions change with time of day, season of year, degree

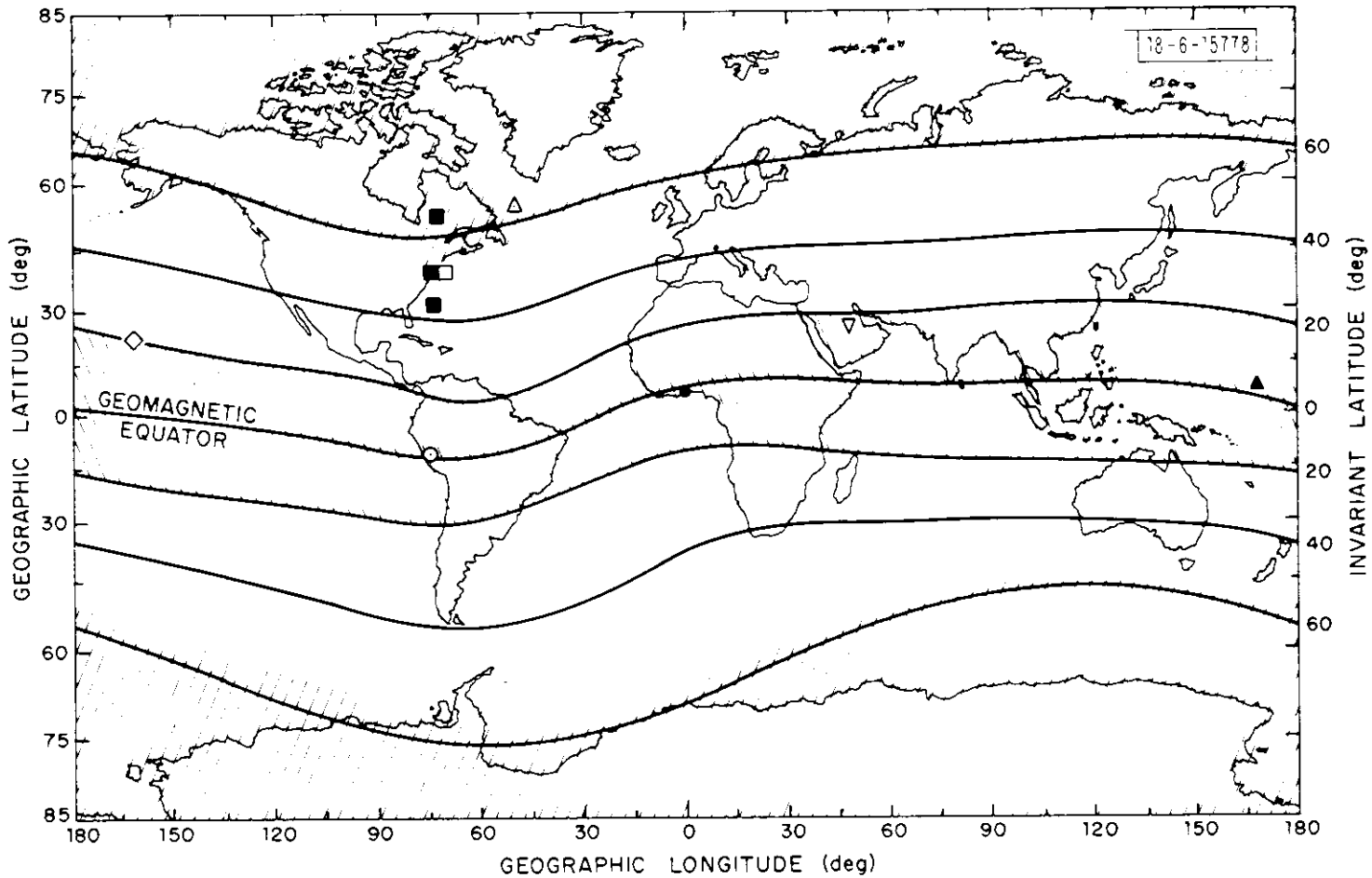

Fig. 16 World map of invariant latitude at a height of 300 km showing sub-ionospheric points of scintillation observations.

of magnetic disturbance, sunspot number and perhaps other geophysical parameters.

Observations of scintillation at 137 MHz using the ATS-3 satellite beacon were reported by Whitney et al.[24, 51] for receivers located in each of the important scintillation regions. The empirical distribution functions for observations from Narssarsuaq, Greenland; Hamilton, Mass.; and Huancayo, Peru, are given in Fig. 17. The locations of the 300-km sub-ionospheric points for each of the receiver sites are shown on Fig. 16. The demarcation line between weak and strong scintillation at σ_X = 2 dB was chosen to coincide with the σ_X value on Fig. 5 at which the Nakagami-m distribution curve begins to veer from the weak scintillation limit line. Optical scintillation observations also show weak scintillation theory to be valid for σ_X values less than about 2-dB.[52] Using the 2-dB value as a bound, strong scintillation was observed 14% of the two-year observation period at $\Lambda = 1°$, 29% of the four-year period at $\Lambda = 64°$, and 2.4% of the three-year period at $\Lambda = 53°$. The mid-latitude-auroral region boundary site suffered strong scintillation approximately an order of magnitude less often than at either the auroral or equatorial sites.

The empirical distribution functions of scintillation intensity reported by Whitney et al. were compiled from extreme value scintillation index data obtained using 15-minute sampling intervals. The scintillation index was

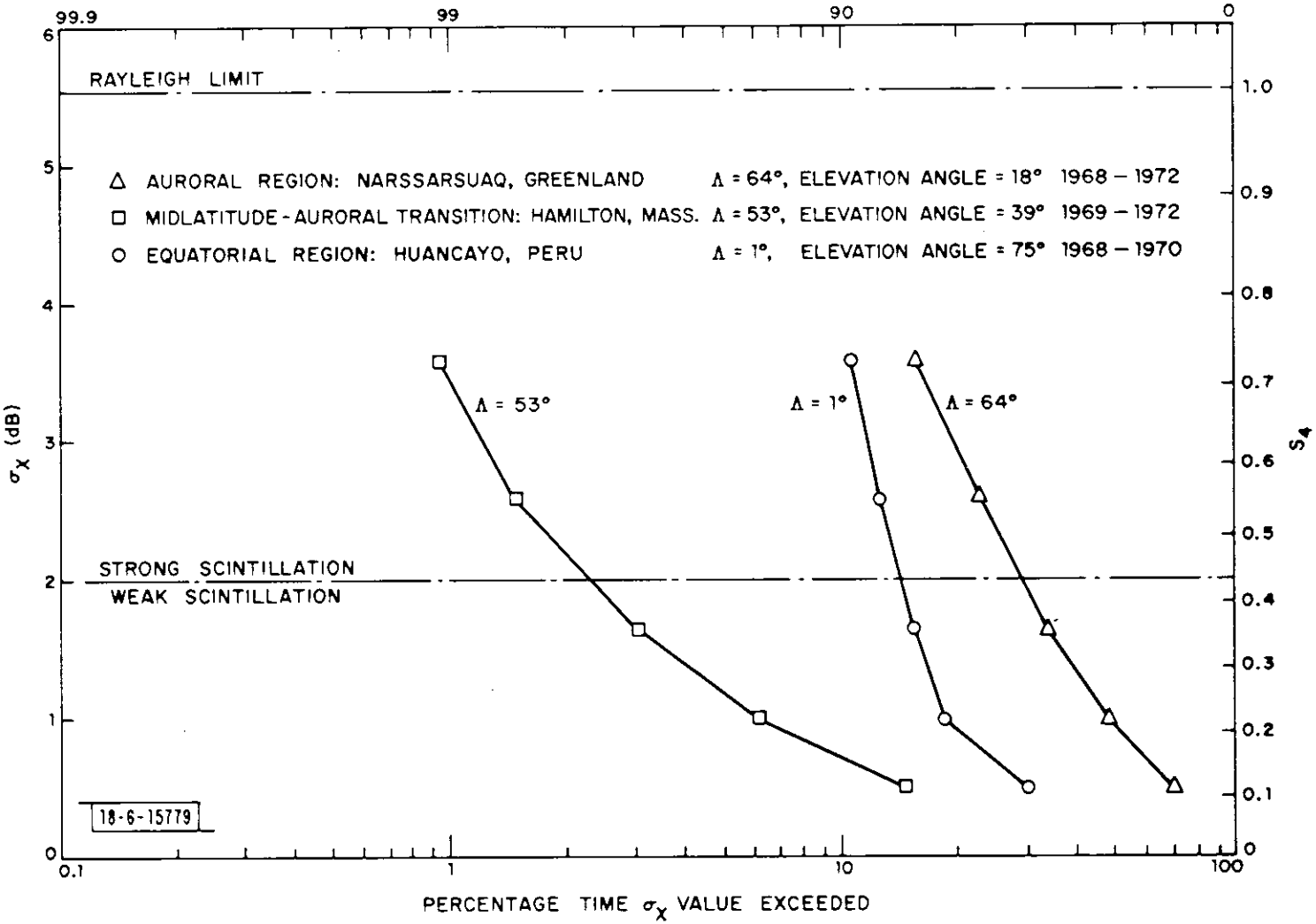

Fig. 17 Empirical distribution function for 137 MHz observations reported by Whitney et al. (Ref. 24, 51).

calculated using the third highest and third lowest recorded power levels within the 15-minute interval. This index may be related to either σ_χ or S_4 only when the received power distribution function is known and when the number of independent samples in an observation interval is known. Using the Nakagami-m distribution, the fading depth and range of received signal levels exceeded by a specified percentage of the independent samples (fading range) may be related to σ_χ as shown in Fig. 18. The scintillation index, SI, is derived from the fading range and is also dependent upon the number of independent samples. S_4 and SI may be related to σ_χ using the Nakagami-m distribution as shown in Fig. 19. Although the Nakagami-m distribution only approximates the time distribution function as shown by Bischoff and Chytil[22] and in Fig. 5, it provides a useful means to relate the qualitative measures of scintillation, SI or fading depth, to the quantitative measures, σ_χ or S_4. For the compilation of distribution functions, Whitney et al first accumulated the number of occurrences of scintillation by scintillation group. The scintillation group classes were defined using fixed ranges of SI hence they also depend upon the number of independent samples. The scintillation group classes drawn on Fig. 19 are for the 3.3 - 96.7% SI curve.

The number of independent samples may be approximated by the number of times the irregularities within the first Fresnel zone are changed during an observation period. Using the ratio of the drift rate of the irregular-

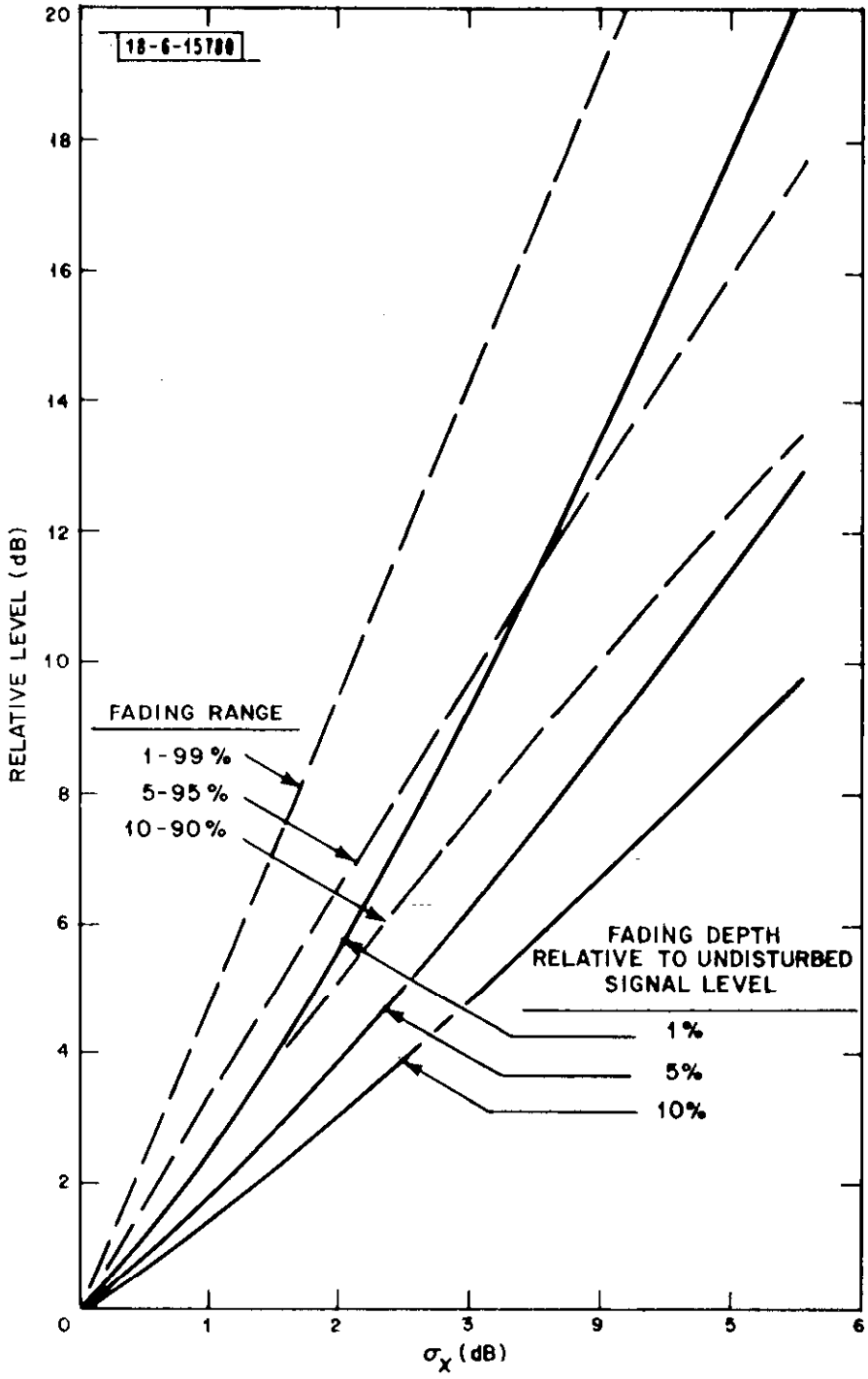

Fig. 18 Fading range and fading depth vs σ_χ for a Nakagami-m distribution.

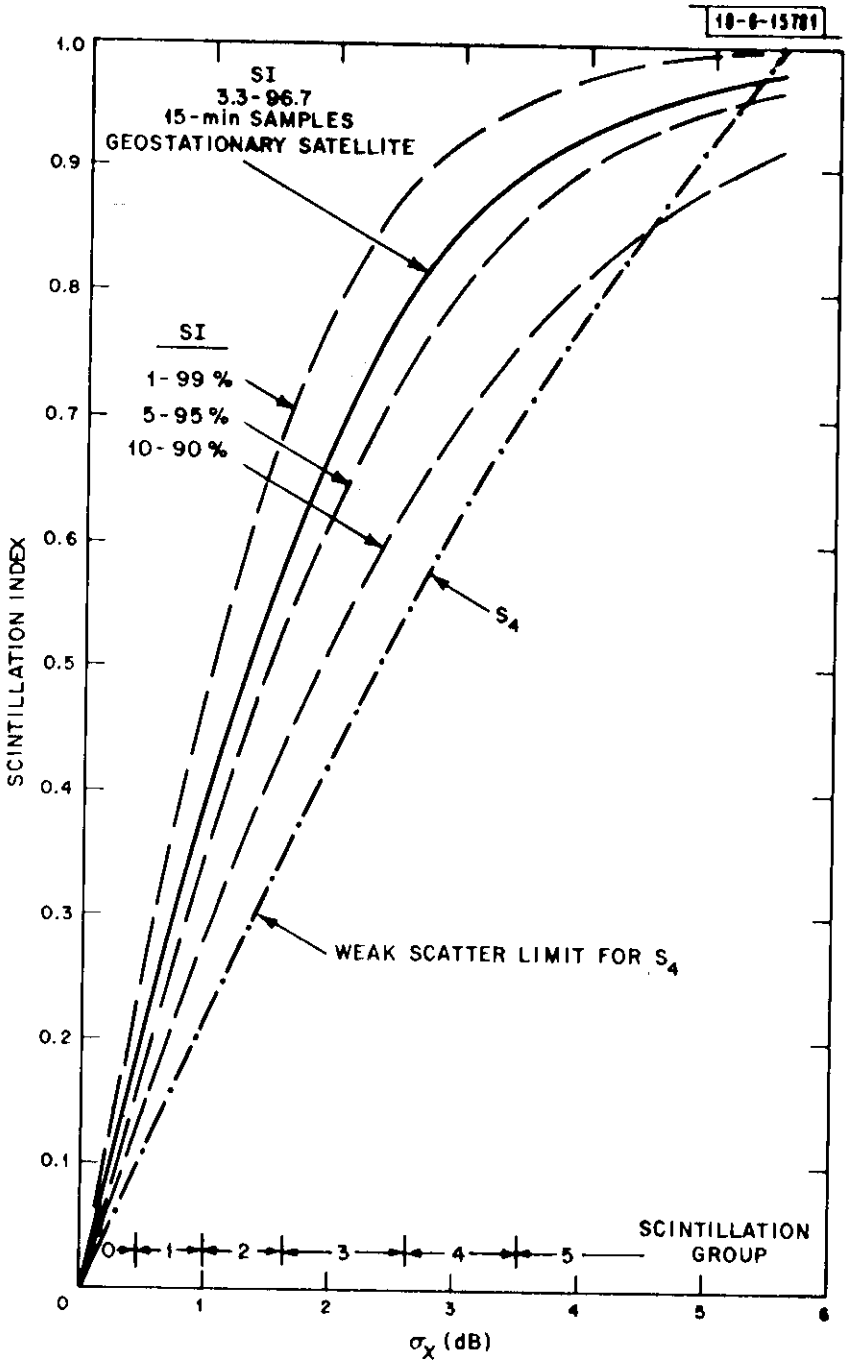

Fig. 19 S_4 and scintillation index (SI) vs σ_χ for a Nakagami-m distribution.

ities through the Fresnel zone to the radius of the first Fresnel zone as an estimate the rate of occurrence of independent samples, the number of samples may be calculated for a given satellite-to-receiver geometry and ionospheric irregularity drift rate. Observations of scintillations from geostationary satellites in the equatorial region yield drift rates typically ranging from 40 to 200 m/sec.[53,54] The calculated first Fresnel zone radius ranges from 0.7 to 1.1 km for 137 MHz, irregularities at a height of 300 km, and elevation angles between 75 and 18°, respectively. Using these values, the number of independent samples observed in 15 minutes may vary from 30 to 300. Fading ranges or SI values calculated using the third highest and third lowest signal levels for the sampling interval therefore correspond to 10-90% for the smaller number of samples and to 1 to 99% for the higher number. The relationship between SI and σ_χ varies over this range of independent samples as shown in Fig. 19. The relationship between SI and σ_χ used to interpret the data of Whitney et al. for display in Fig. 18 is given by the solid curve for 3.3 - 96.7% and corresponds to the use of the mean nighttime drift rate, 70 m/sec, reported by Koster and Katsriku[54] and the 0.7-km Fresnel zone radius appropriate to high elevation angles. Whitney et al. used the median signal level distribution functions obtained for a limited number of observations in each scintillation group to provide an estimate of the median S_4 value for each group. The

1-99% SI curve best fit their results. It is felt, however, that in the absence of better information on drift velocities the relationship based upon an estimate of drift velocity should be used. The maximum error in the estimation of σ_χ caused by using the 3.3 - 96.7% SI curve is 0.2 dB at σ_χ = 1 dB and 0.6 dB at σ_χ = 3 dB.

Elevation Angle Dependence

The distribution functions displayed on Fig. 17 are for roughly the same time periods and for different elevation angles. The scintillations may be caused by electron density fluctuations anywhere along the ray path through the ionosphere. Early studies showed positive correlation between the occurrence of scintillation and the occurrence of spread-F for nighttime scintillation[3, 5, 55, 56, 57] and between the occurrence of scintillation and of sporadic E and spread-E in the mid-latitude region.[55, 56, 57, 58, 59] Studies of the heights of the regions causing nighttime scintillation show that the irregularities may occur over a wide range of heights, 200 to 600 km.[8, 53, 60] Radar data obtained in the equatorial region[16] show that the irregularities occur in one or more layers each of which may be one hundred or more kilometers in vertical extent.

The variance of the logarithm of the received signal level may be calculated in the limit of weak scintillation for a power-law power spectrum with a three-dimensional index P = 4 using the Rytov method:[18]

$$\sigma_\chi^2 \propto \frac{\lambda^3}{2L} \int_{\ell_1}^{\ell_2} \frac{\alpha \sigma_N^2(\rho)(1 + \cos^2\Psi + \alpha^2 \sin^2\Psi)\rho(L-\rho)d\rho}{(\cos^2\Psi + \alpha^2 \sin^2\Psi)^{3/2}} \qquad (1)$$

where

$\sigma_N^2(\rho)$ = variance in electron density at point ρ along the ray

Ψ = angle between the direction of propagation and the magnetic field (propagation angle)

α = axial ratio of the irregularities (see Ref. 13)

L = distance to satellite along the ray

ℓ_1, ℓ_2 = integration limits for the ionospheric irregularities along the ray.

If α and Ψ do not change along the ray, for $L >> \ell_2$, for propagation above a flat earth (useful for elevation angles above 10°), and for $\sigma_N^2(\rho)$ constant between, ℓ_1 and ℓ_2

$$\sigma_\chi \propto \lambda^{3/2} f(\Psi, \alpha) \frac{\sqrt{HD}}{\sin\theta} \left[1 - \frac{H}{L} - \frac{D^2}{12\,HL}\right]^{1/2} \cong \lambda^{3/2} f(\Psi, \alpha) \frac{\sqrt{HD}}{\sin\theta} \qquad (2)$$

where

$$f(\Psi, \alpha) = \left[\frac{\alpha(1 + \cos^2\Psi + \alpha^2 \sin^2\Psi)}{2(\cos^2\Psi + \alpha^2 \sin^2\Psi)^{3/2}}\right]^{1/2}$$

H = height of the center of a thick irregularity layer

D = thickness of the layer

θ = elevation angle

It is noted that the dependence of σ_χ on elevation angle, propagation angle, and axial ratio calculated for the power law power spectrum with an index of 4 is different from the dependence calculated by Briggs and Parkin[13] for the Gaussian correlation function case ($S_4 \propto \sigma_\chi$ in the weak scintillation limit).

Observation of the elevation angle dependence of scintillation is difficult due to the accompanying geographic variation of scintillation. The data taken at Millstone were obtained from observations of low orbiting satellites. The elevation angle of the ray path to the satellite varied during the satellite pass and the geographical location of the irregularity region along the ray at a particular elevation angle varied from pass to pass. During the 1971-1973 time period, 2376 satellite passes were observed.[62] The observations were made during two-to-three day tracking session at two-to-three week intervals. The Millstone data were taken at random over all times of day, seasons, and variations of geophysical activity. Although not continuous, the data represent a random sample of scintillation activity. For statistical analysis, the UHF power fluctuations (S_4 values) were tabulated for successive three-second intervals along each pass. To evaluate the elevation angle dependence of scintillation, the data were stratified by invariant latitude and elevation angle. A sample of the observations for $60° \leq \Lambda \leq 62°$ is shown in Fig. 20. The data points are from the individual

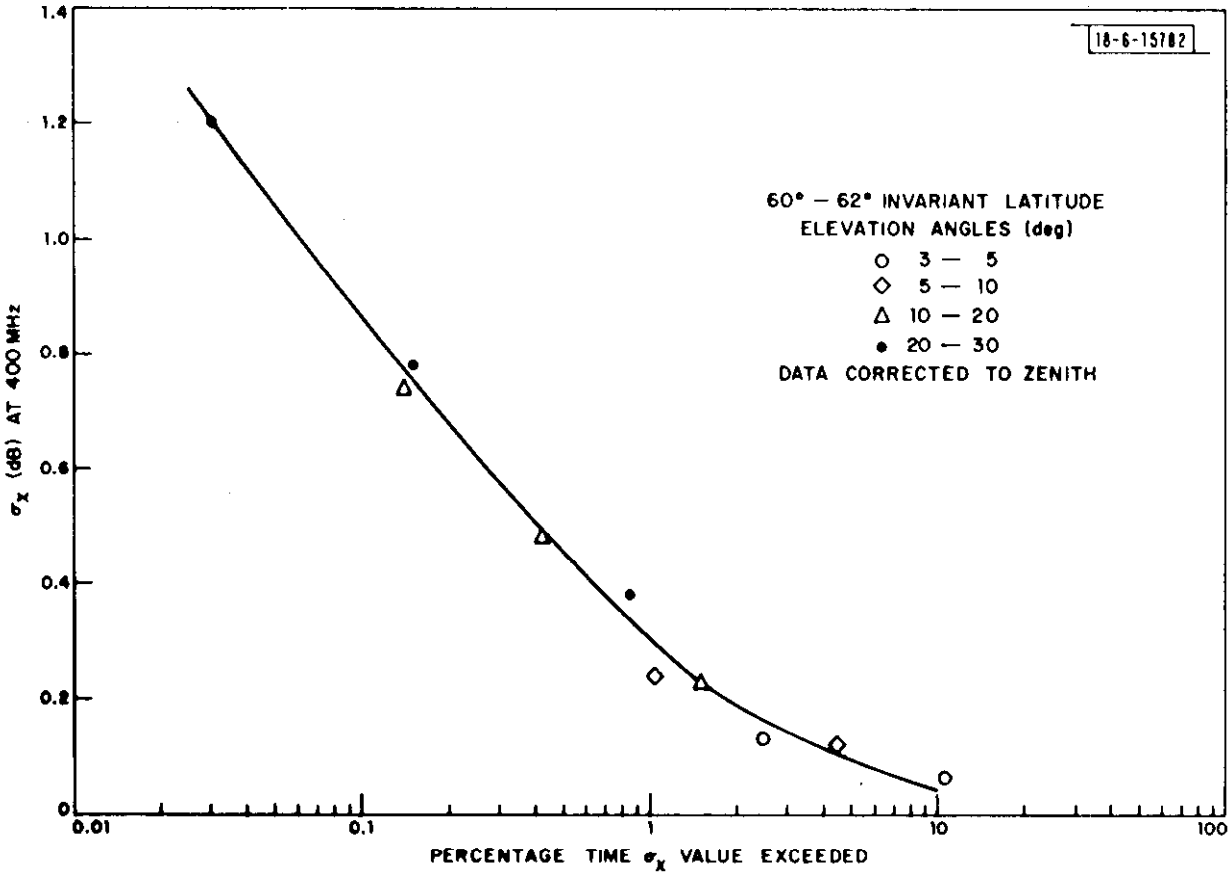

Fig. 20 Zenith corrected empirical distribution function for 400-MHz Millstone observations at several elevation angles.

distribution functions for specified elevation angle ranges normalized to zenith using Eq. (2). The curve is drawn to approximate a median distribution function for the range of elevation angles used. The maximum errors are 40% in percentage occurrence (or .05 dB in σ_χ). Using the elevation angle dependence recommended by Briggs and Parkin (Gaussian correlation function), the maximum deviations from the best fit median distribution function was 200% (or .5 dB in σ_χ). The elevation angle dependence specified by Eq. (2) therefore is significantly better than for the Guassian correlation function model. Data obtained for invariant latitudes between 56° and 68° produced similar results, errors less than 40% in percentage occurrence between the best fit curves and the observed distribution function values. For invariant latitudes below 56° the sample size was small and the errors increased (see Fig. 21 for the range of observations for $52° < \Lambda < 54°$). For these invariant latitudes, the Gaussian correlation function model again was singificantly poorer.

The regional variation of the occurrence of scintillation is best described using estimated zenith σ_χ values with the elevation angle and propagation angle dependence removed using Eq. (2). For most recorded observations, the propagation angle and axial ratio values are not known. The correction factor $f(\Psi, \alpha)$ is unity if $\alpha = 1$ and ranges from $\sqrt{\alpha}$ to 0.7 as a function of Ψ for $\alpha > 1$. For $\Psi = 0°$ (propagation along a field line)

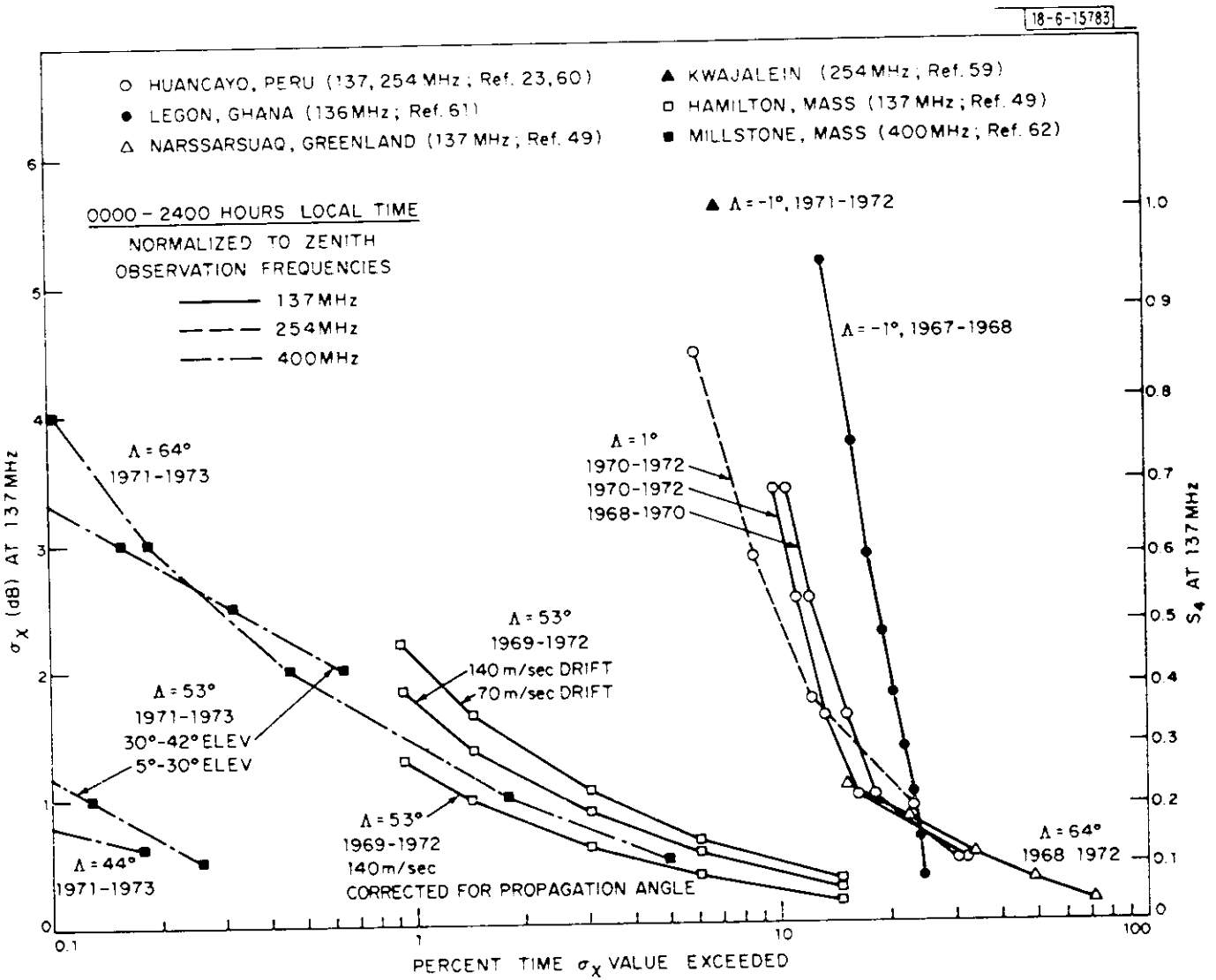

Fig. 21 Zenith corrected empirical distribution functions for 137 MHz.

$f(\Psi, \alpha) = \sqrt{\alpha}$ for all values of α. The most rapid change of $f(\Psi, \alpha)$ with α occurs at a propagation angle $\Psi = 0°$. The propagation angles for the ATS-3 observations were 80° for Huancayo, 154° for Hamilton, and 124° for Narssarsuaq.[51] Information about typical axial ratios is sparse. Data from both equatorial and auroral regions indicate that the axial ratios are greater than 5.[8,53] For an axial ratio of 5, the correction factors are 0.73, 1.12 and 0.8, respectively. Since the correction factors are nearly the same for each set of observations and the results differ appreciably from 0.8 only for propagation within 40° of the field line, the geometrical variation of σ_χ may be expressed as

$$\sigma_\chi \propto \frac{\lambda^{3/2}\sqrt{HD}}{\sin\theta} \tag{3}$$

Zenith path estimates of the occurrence of scintillation obtained using Eq. (3) and the data in Fig. 17 are shown in Fig. 21. Additional distribution function estimates obtained by scaling higher frequency data using Eq. (3) are also included. The 400-MHz observations were made at Millstone both to the north of the station ($\Lambda = 64°$) and to the south ($\Lambda = 53°$ and 44°) and have been scaled to extend the auroral and mid-latitude observations. For $\Lambda = 53°$, data scaled from measurement angles above and below 30° are separately displayed. A comparison of the data above and below 30° shows either a propagation angle dependence or the effect of a limited sample size. Hamilton distribution functions ($\Lambda = 53°$) generated by using two separate drift velocity assumptions are displayed. These distribution functions

differ from the Millstone below 30° distribution function by an order of magnitude in percentage occurrence. The 140 m/sec drift rate, elevation angle greater than 30° curves, however, are in agreement indicating that the discrepancy may be caused by the propagation angle. A third curve for Hamilton is also shown on the figure for 140 m/s drift velocity and a propagation angle correction calculated using Eq. (2). Similar propagation angle corrected data with a sufficient sample size to be statistically significant are not available for Millstone. The drift velocity, propagation angle corrections do however improve the comparison between the Hamilton observations and the Millstone below 30° observations. The remaining discrepancy is most likely due to the limited sample size of the Millstone data for invariant latitudes below 54°.

Data obtained at 254 MHz from Kwajalein[63] and from Huancayo[64] together with additional 137 MHz data from Huancayo and Legon, Ghana,[65] are also included in Fig. 21. The locations of the additional observations are shown on Fig. 16. The zenith path occurrence estimates show that scintillation is far more severe in the equatorial region than in either the auroral or mid-latitude regions. Using these observations, strong scintillation ($\sigma_X > 2$ dB) occurs between 10 and 20% of the time in the equatorial region, between 1 and 2% of the time in the auroral region and less than 1.0% of the time in the mid-latitude region for the stations used and for the

1967-1972 time period.

The data also seem to show that scintillation occurs more often at geographic longitudes near 0° than at 75°W or 165°E for sites near the geomagnetic equator. The data are of limited accuracy due to the use of qualitative scaling procedures. The Legon distribution function was compiled using five-minute sampling intervals and the 10-90% SI curve on Fig. 19. The uncertainty caused by not knowing the applicable drift rate may be as much as 0.5 dB for σ_χ near 2 dB. This uncertainty may reconcile the several observations at Huancayo but is not large enough to reconcile the difference between the Huancayo and Legon observations. The Kwajalein observations included a distribution function value estimate at $\sigma_\chi = 5$ dB. This value could not be included with the 137-MHz estimates because of the σ_χ limit value of 5.6 dB (see Fig. 14). The 137-MHz observations can be used to estimate the occurrence probabilities of scintillation at 254 MHz as shown on Fig. 22. The differences in occurrence probability at the separated equatorial sites is again evident. Since the 137-MHz data were generally for weak scintillation, the scaling to 254 MHz is permissible although the estimates are only for very weak scintillation. The higher σ_χ values for the Legon data may be in error due to strong scintillation at 137 MHz. Two single values scaled from 4000-MHz observations[10] from stations near the equatorial-mid-latitude region boundary indicated by the same symbols on

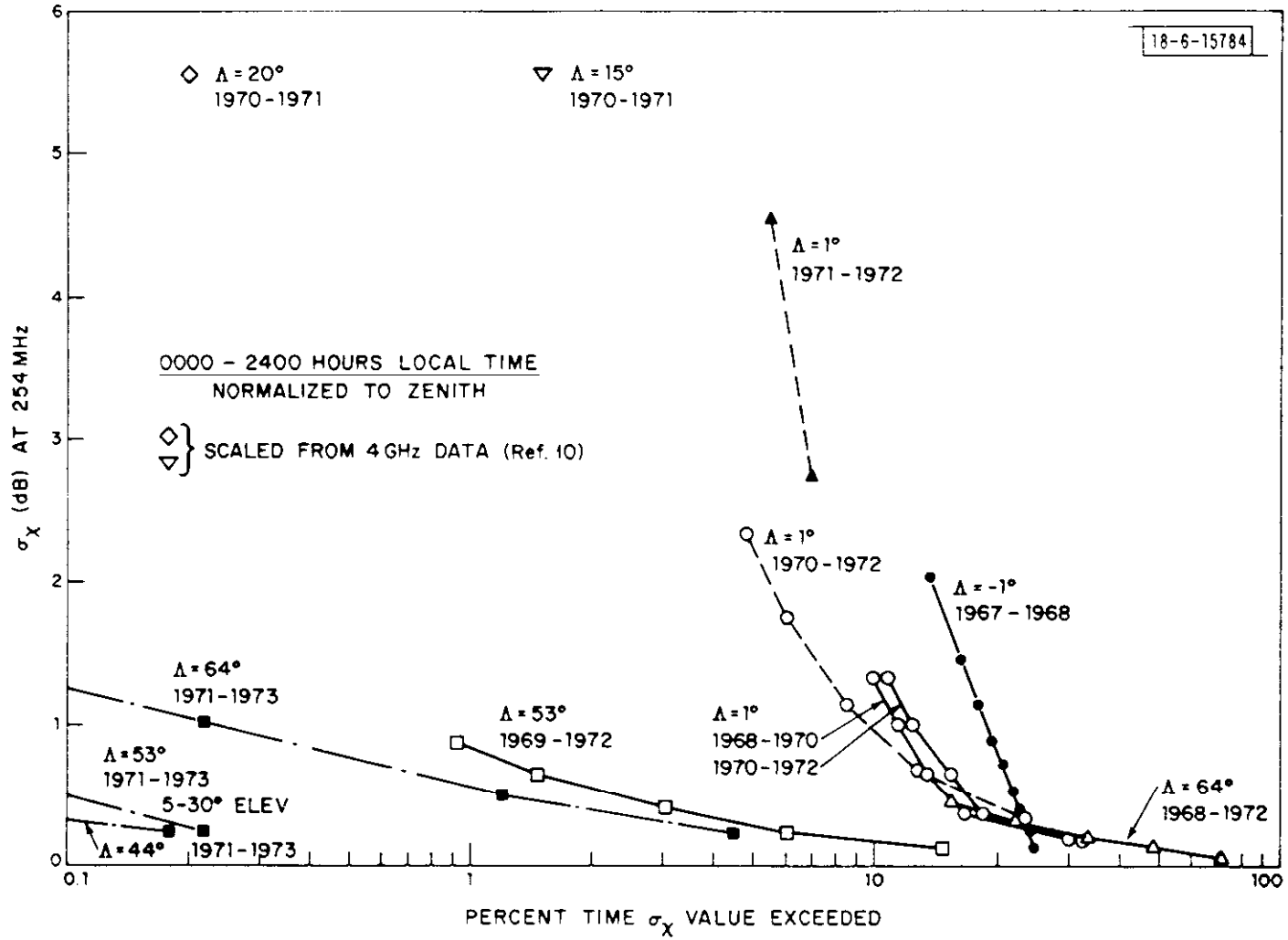

Fig. 22 Zenith corrected empirical distribution functions for 254 MHz.

Fig. 16 are also included. These data points correspond to just detectable scintillation (. 9 dB peak-to-peak) at 4000 MHz. The 254-MHz estimates show that strong scintillation ($\sigma_\chi > 2$ dB) occurs for less than 15 percent of the time on a zenith path in the equatorial region, 0. 2 percent in the auroral region and less than 0. 1 percent at a mid-latitude site. For a path at a 20° elevation angle, the percentage of occurrence values increases to 25 percent in both the auroral and equatorial regions and between 1 and 6 percent at mid-latitudes.

Latitude Variation

Empirical distribution functions scaled from observations made within each scintillation region are shown in Figs. 21 and 22. The data shown on Fig. 22 for Λ = 15° and 20° show nearly an order of magnitude change in percent occurrence within 4° invariant near the mid-latitude, equatorial region boundary. The Λ = 53° data is also for a transition zone between the auroral and mid-latitude region. These data appear to have higher probabilities of occurrence of scintillation than data for Λ = 44°, a location well within the mid-latitude region. Low orbiting satellite data have also been analyzed to depict latitudinal variation. The 400-MHz Millstone observations were compiled to yield occurrence data for 2° invariant latitude intervals as shown in Fig. 23.[62] The data in Fig. 23 were not corrected for elevation angle. If the occurrence probabilities were inde-

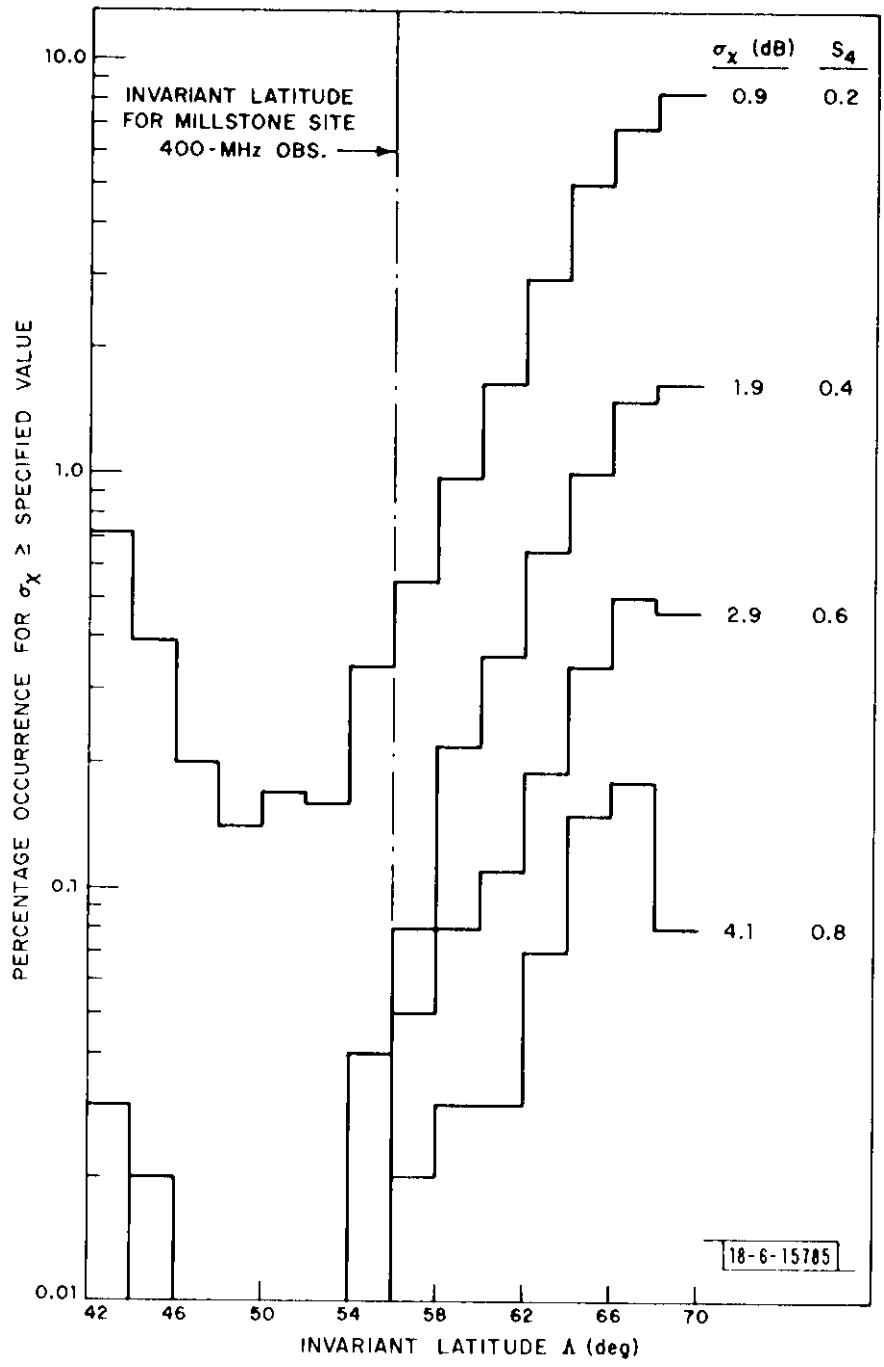

Fig. 23 Percentage occurrence of σ_χ vs invariant latitude at 400 MHz for the Millstone observations.

pendent of Λ, the curves would by symmetrical about 56°. The relative increase towards the north (higher Λ values) indicates that scintillation occurs most often in the auroral region. Figure 24 shows Millstone data corrected for elevation angle and scaled to σ_χ values at 137 MHz. These data show a relatively constant probability of occurrence of strong scintillation to the north of $\Lambda = 56°$ and constant but significantly lower occurrence to the south.

The latitudinal variation of scintillation has been studied using low orbiting satellites and frequencies between 40 and 54 MHz.[61, 66, 67, 68] The data showed the same asymmetry for propagation to the north and south of stations near $\Lambda = 55°$ as shown in Fig. 23. Unfortunately, most of the data were reported as averages of the scintillation index which are not useful in estimating probabilities of occurrence. Data at 40 MHz are also not useful in estimating the occurrence of scintillation index at UHF because measurable SI values at 40 MHz ($SI_{3.3-96.7\%} = .6$ (60%)) correspond to very low values of σ_χ ($\sigma_\chi = 0.3$ dB at 137 MHz and $\sigma_\chi = 0.1$ dB at 254 MHz). 40-MHz data from three stations in the equatorial region[69] show that the percentage occurrence of scintillation is reasonably constant within 5°Λ of the magnetic equator, falls off by a factor of 2 at 10° and by a factor of 4 at 15°. The equatorial distribution function estimates plotted on Fig. 22 show a similar behavior.

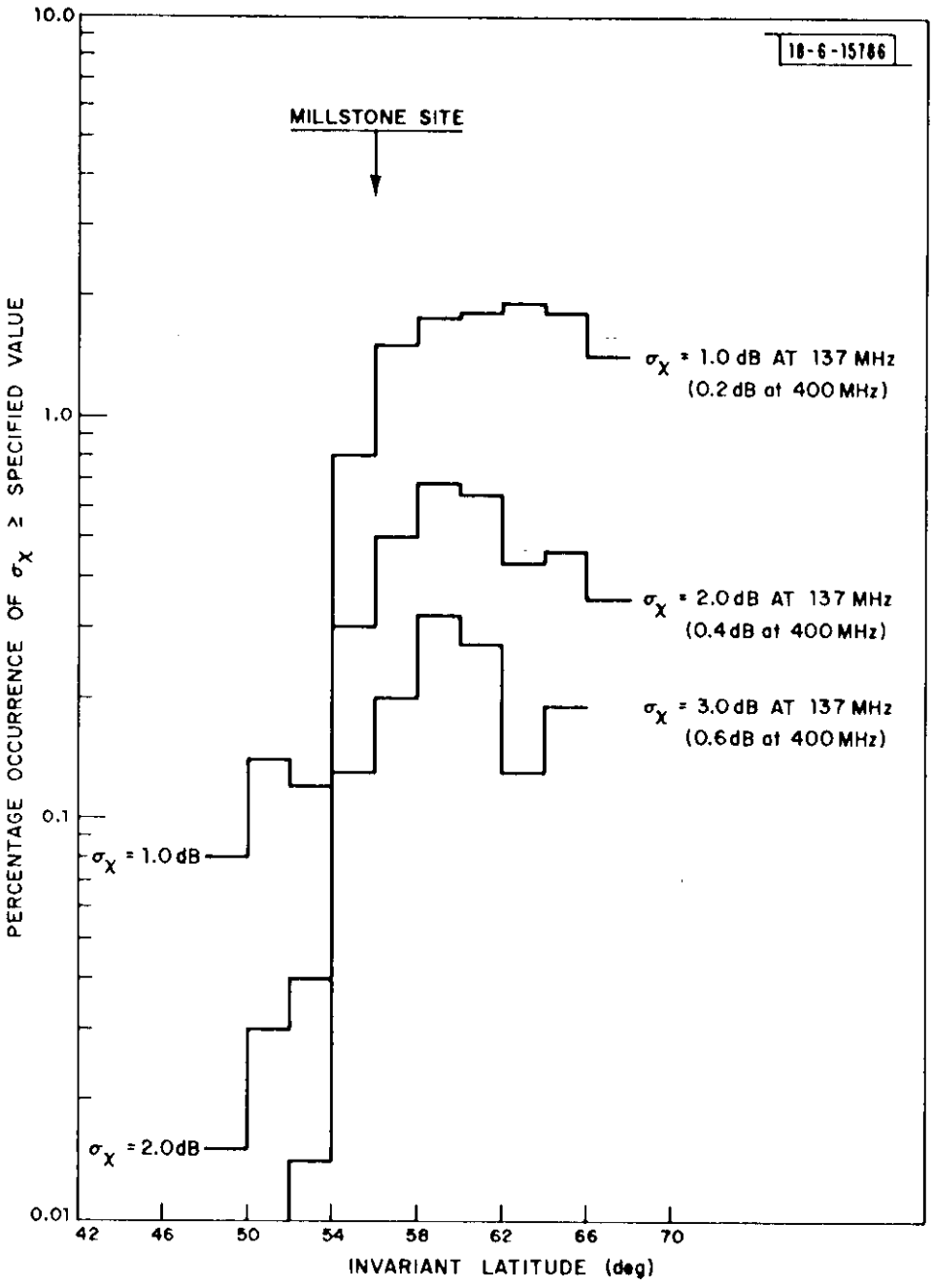

Fig. 24 Zenith corrected percentage occurrence of σ_χ vs invariant latitude for the Millstone observations.

Observations at 40 and 54 MHz near the mid-latitude-auroral region boundary generally show a sharp boundary between scintillation activity in the auroral region and the relatively quiet mid-latitude region.[3, 70, 71] The abrupt change in the percentage occurrence of scintillation is also indicated in Fig. 24. Abrupt changes at an apparent scintillation boundary are also evident in the Millstone data shown in Fig. 25 (replotted from Fig. 3 as a function of Λ). Aarons et al. have defined a scintillation boundary as the latitude at which SI at 40 MHz is 0.5 (50%). Scintillation activity of such a level is too weak to be detected at 400 MHz and the Millstone boundary data may not coincide with the location defined by Aarons et al. Boundaries between regions of high and low scintillation activity are also evident in equatorial observations. The equatorial fluctuations are often described as starting abruptly and ending as quickly. The data reported by Koster[8] show scintillation occurring in patches that have East-West dimensions ranging from 100 to 700 km.

Diurnal Variation

Data from the auroral and equatorial regions show distinctly different variations with time of day. The diurnal variation in the percentage occurrence of strong scintillation at 137 MHz for zenith corrected observations for each of the scintillation regions is shown in Fig. 26. The equatorial data are from Legon ($\Lambda = -1°$)[65] and Huancayo ($\Lambda = +1°$).[24, 63] The mid-

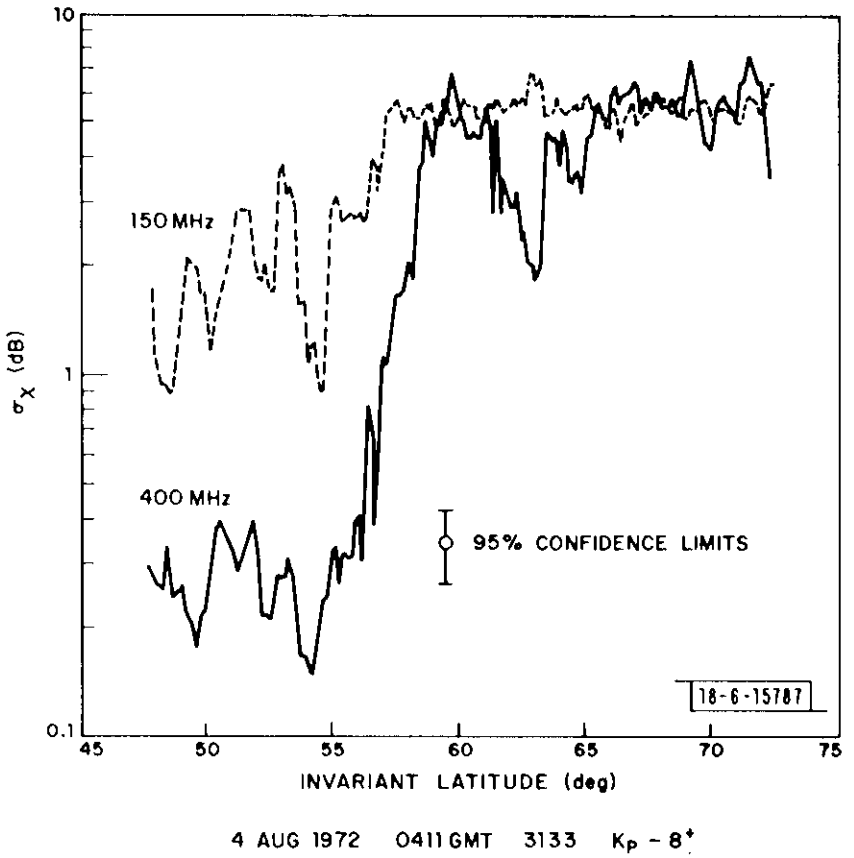

Fig. 25 Latitude dependence of scintillation for pass of Object #3133 rising at 0411 GMT 4 August 1972 (Kp = 8^+).

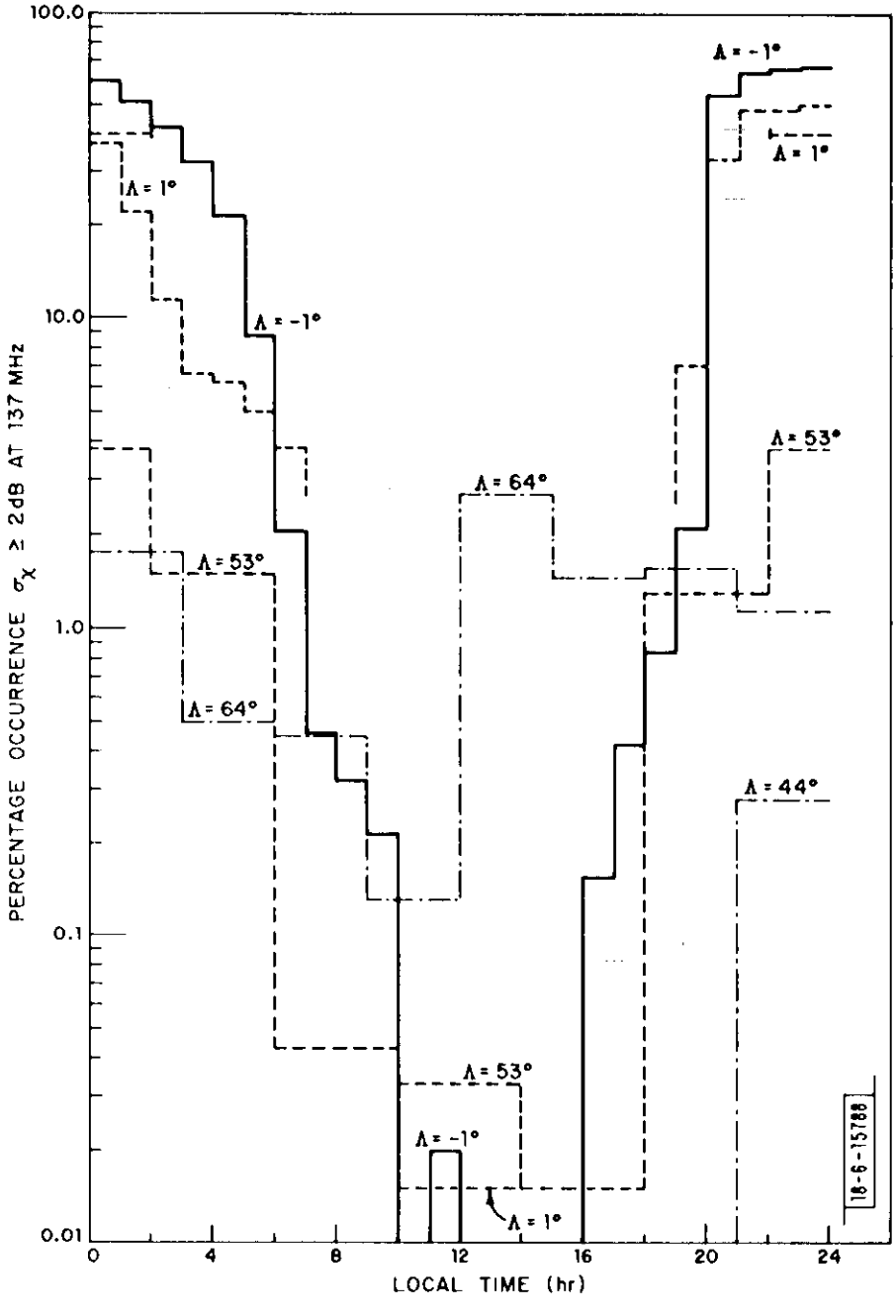

Fig. 26 Percentage occurrence of σ_χ local time.

latitude data are scaled from the 400 MHz Millstone data ($\Lambda = 44°$). The data for $\Lambda = 53°$ are from Hamilton, Mass.[49] The auroral region data are scaled from 400-MHz Millstone data ($\Lambda = 64°$). The Narssarsuaq data were taken at too low an elevation angle for use in estimating strong scintillation ($\sigma_\chi \geq 2$ dB) on a zenith path. The observations show that scintillation is predominantly a nighttime phenomenon at equatorial and mid-latitudes and may occur during the day or evening in the auroral zone. The predominantly nighttime occurrence of scintillation was also noted for Kwajalein where only two occurrences of $\sigma_\chi \geq 3$ dB at 254 MHz were observed for the hours between 0800^h and 1900^h local time. To further illustrate the diurnal variation, the distribution functions for the several observing stations are given in Fig. 27 for a four-hour period bracketing local midnight and in Fig. 28 for a four-hour period bracketing local noontime.

The nighttime data show that strong scintillation occurs between 30 and 60 percent of the time in the equatorial region and less than 10 percent of the time in the auroral region. The Millstone data for the auroral region seems to show a singificantly smaller probability of occurrence than the Narssarsuaq data for the same invariant latitude or for the Hamilton data for the auroral, mid-latitude region transition. This may be due to the small difference in longitude at the subionospheric point or, more likely, to the difference in the propagation geometry, the Millstone observations were made looking to

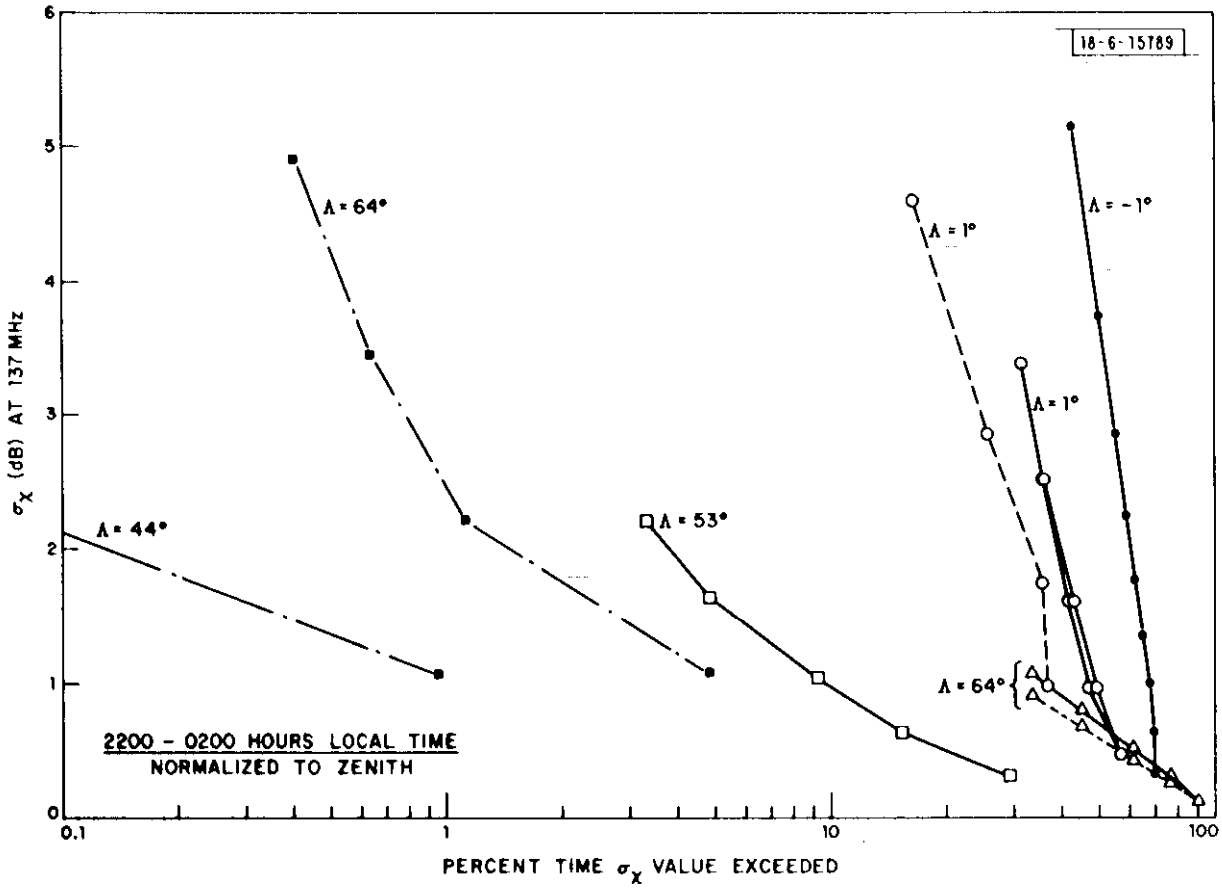

Fig. 27 Zenith corrected empirical distribution functions for 137 MHz and 2200-0200 local time.

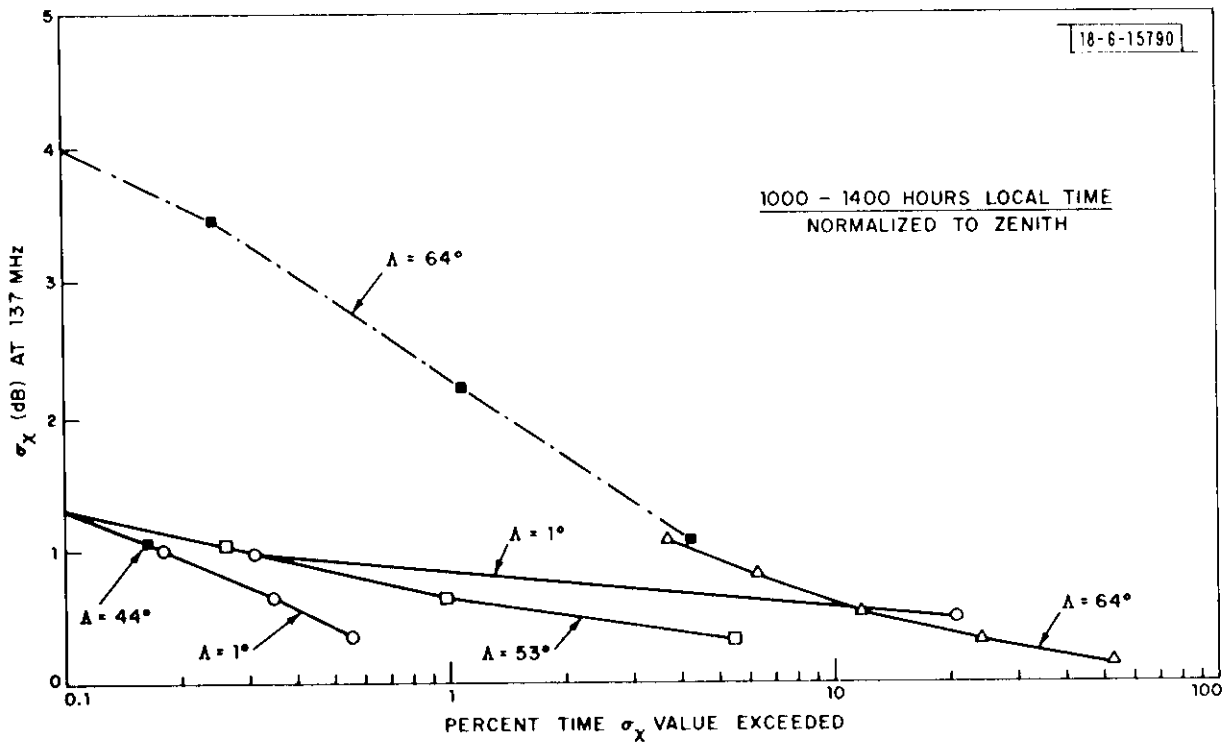

Fig. 28 Zenith corrected empirical distribution functions for 137 MHz and 1000-1400 local time.

the north and the Narssarsuaq and Hamilton observations toward the south. The effect of the variation in propagation angle (see Eq. (2)) is however not sufficient to explain the difference. The difference is not due to elevation angle since the Millstone and Narssarsuaq observations were made at approximately the same elevation angle. The uncertainty in drift velocity for the Narssarsuaq data may contribute, in part, to the apparent discrepancy. Assuming a drift velocity of 200 m/sec, the curve would be changed to the dotted line on Fig. 27. This change in not sufficient to explain the difference. The daytime data show little scintillation activity except at auroral latitudes. In this case, the Millstone and Narssarsuaq are in agreement.

Seasonal Fluctuations

Data from the auroral and equatorial regions show distinctly different seasonal variations. The seasonal variation of strong scintillation at 137 MHz for zenith corrected observations is shown in Fig. 29. The data display the relative orders of magnitude of occurrence for auroral (Λ = 53° and 64°), equatorial (Λ = -1°) and mid-latitude (Λ = 44°) scintillation. The equatorial data for 1967-1968 show maxima near the equinoxes and minima near the solstices. Koster[8] summarized three more years of observations 1968-1971 and found relatively high values near the eqinoxes for each of the years, a pronounced minimum at the northern solstice (June)

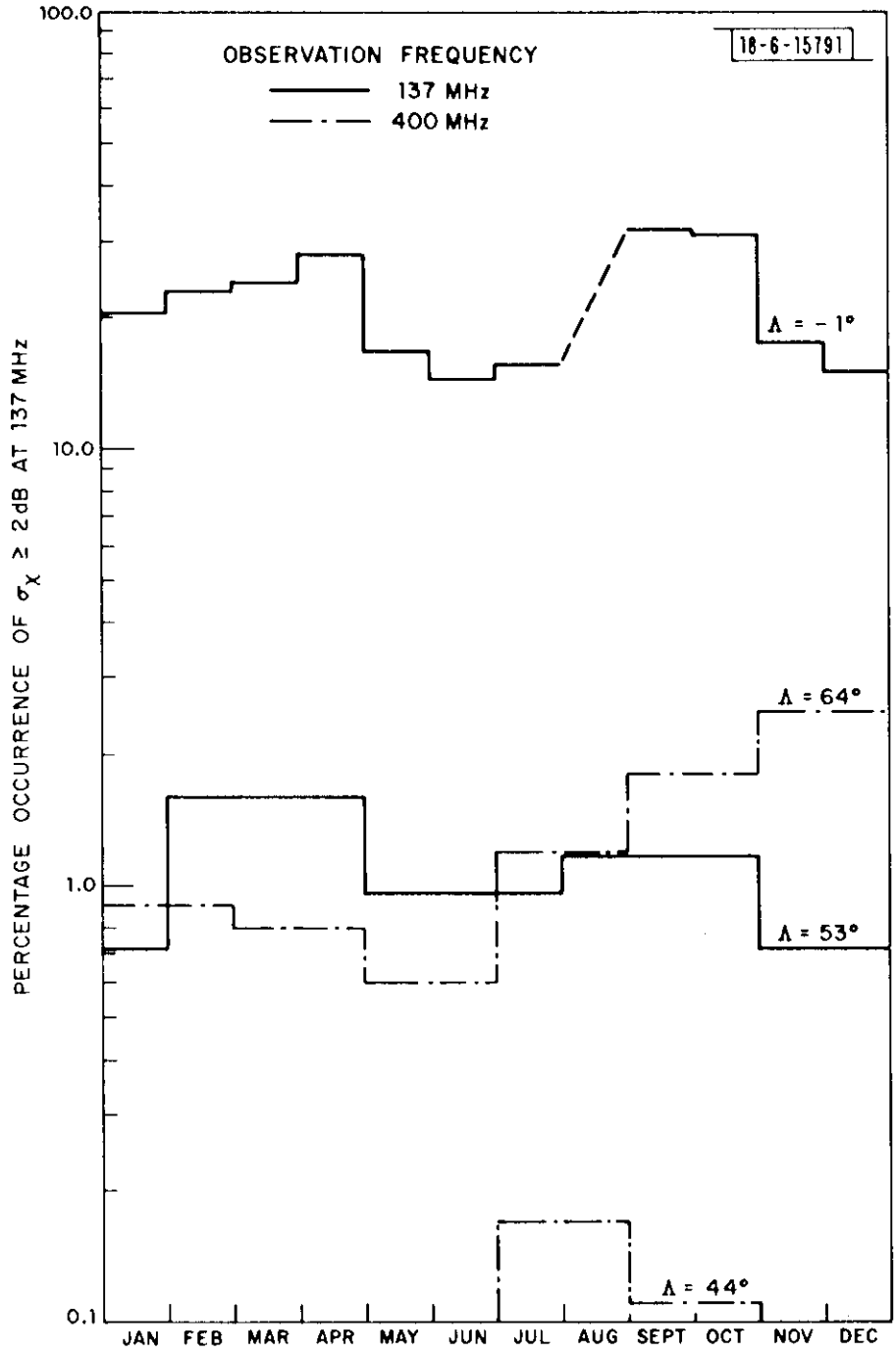

Fig. 29 Zenith corrected percentage occurrence of σ_χ vs month of year.

and a secondary minimum at the southern solstice (Nov.-Jan. depending upon the year). The seasonal variation of the 254-MHz equatorial observations made at Kwajalein is depicted in Fig. 30. For this site, the pronounced minimum is at the southern solstice and the secondary minimum (weak) is at the northern solstice. A similar seasonal behavior for equatorial spread-F has been noted by Davis[72] for a year with high sunspot numbers. The auroral and mid-latitude site data do not show as consistent a seasonal variation as do the equatorial station data.

Dependence on Geophysical Activity

Studies of the dependence of scintillation on geophysical activity have shown that scintillation tends to occur more often during years with high sunspot number[3, 8, 70] and, in the auroral region to have a strong dependence on magnetic activity.[3, 71] The data displayed in Figs. 21 and 22 are primarily for high sunspot numbers, the smoothed Zurich sunspot numbers R_z were greater than 90 from June 1967 (start of Koster's observations[65]) to November 1970. The data of Koster (1967-1968) had an average $R_z = 102$. The 1970-1972 data had a lower average value, $R_z = 72$. The 137-MHz data displayed on Fig. 21 for Huancayo show only small differences for the two data sets, 1968-1970 and 1970-1972, although the set for the smaller R_z value had lower probability of occurrence for a fixed σ_X level (14% vs 12.5% for $\sigma_X = 2$ dB) and a lower σ_X value for a fixed percentage

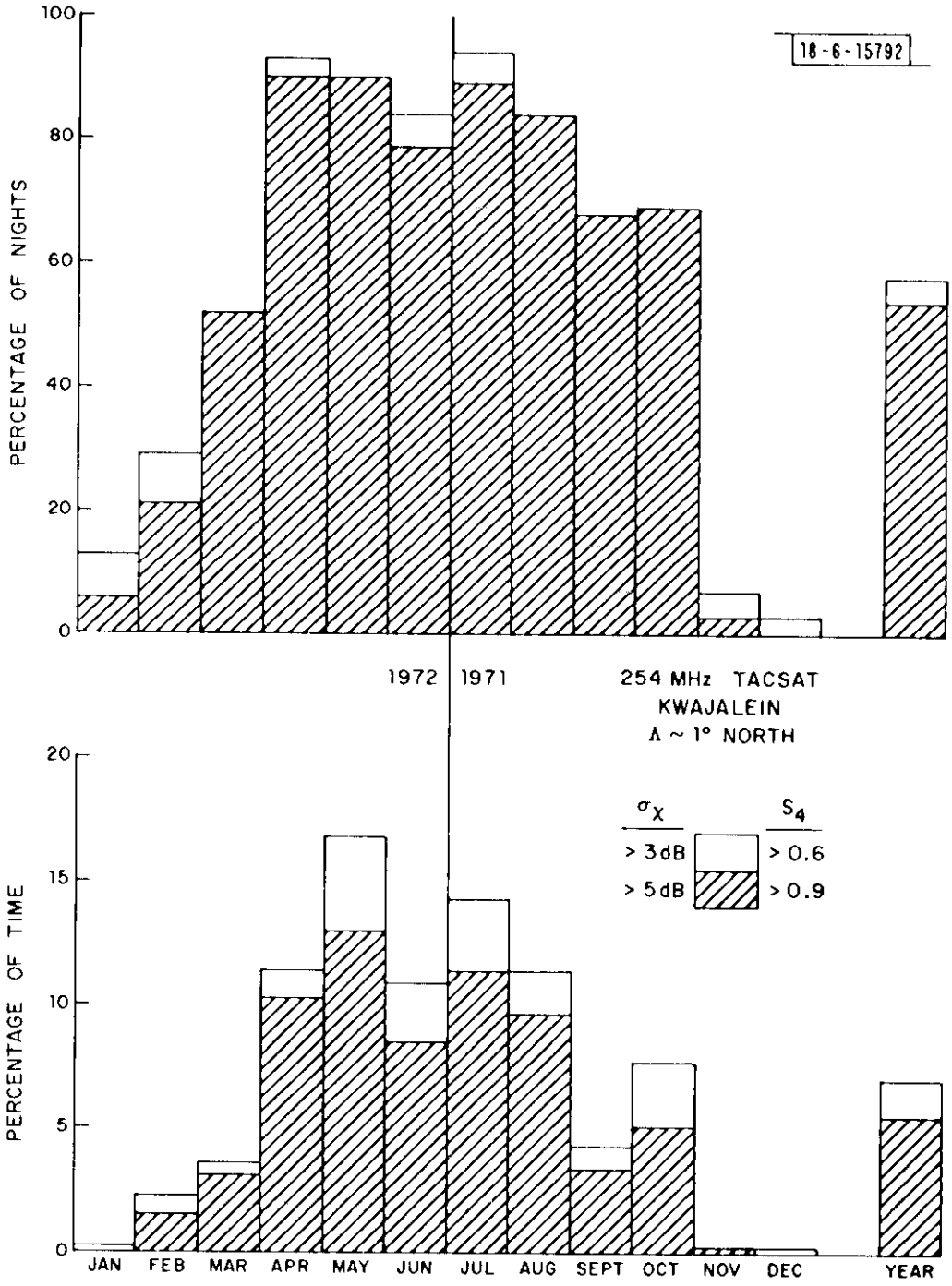

Fig. 30 Zenith corrected percentage occurrence of σ_χ vs month of year for Kwajalein ($\Lambda = +1^0$).

occurrence (1.7 vs 1.3 dB at 15%, nearly the same ratio as for R_z). The data for nighttime occurrence, Fig. 27 however did not show any dependence of σ_χ or percent occurrence on R_z. The Kwajalein data were for $R_z = 66$, considerably lower than the R_z value for Legon, Ghana. The data show a trend towards σ_χ or percent occurrence increasing as R_z increased but insufficient data are available to determine a precise dependence.

Auroral region scintillation show a strong dependence upon magnetic activity, K_p. 400-MHz Millstone data for the auroral region, $\Lambda = 64°$, and the mid-latitude region, $\Lambda = 44°$, are given in Fig. 31. The data are for nearly identical elevation angles and are not zenith corrected. A high correlation of σ_χ with K_p and of the latitude of the scintillation boundary with K_p have been reported by Aarons.[71] The dependences of the percentage occurrence of σ_χ on K_p for auroral and mid-latitude regions are shown in Fig. 31. The dependence of equatorial scintillation on K_p is weak. Both positive and negative correlations of scintillation with K_p have been reported. The results seem to depend upon longitude and sunspot number.

Temporal Behavior of Scintillation

The occurrence probability information compiled above were obtained from 5- to 15-minute samples of data from geostationary satellites or three-second samples of data from low orbiting satellites. Strip chart recordings of scintillation from geostationary satellites typically show long

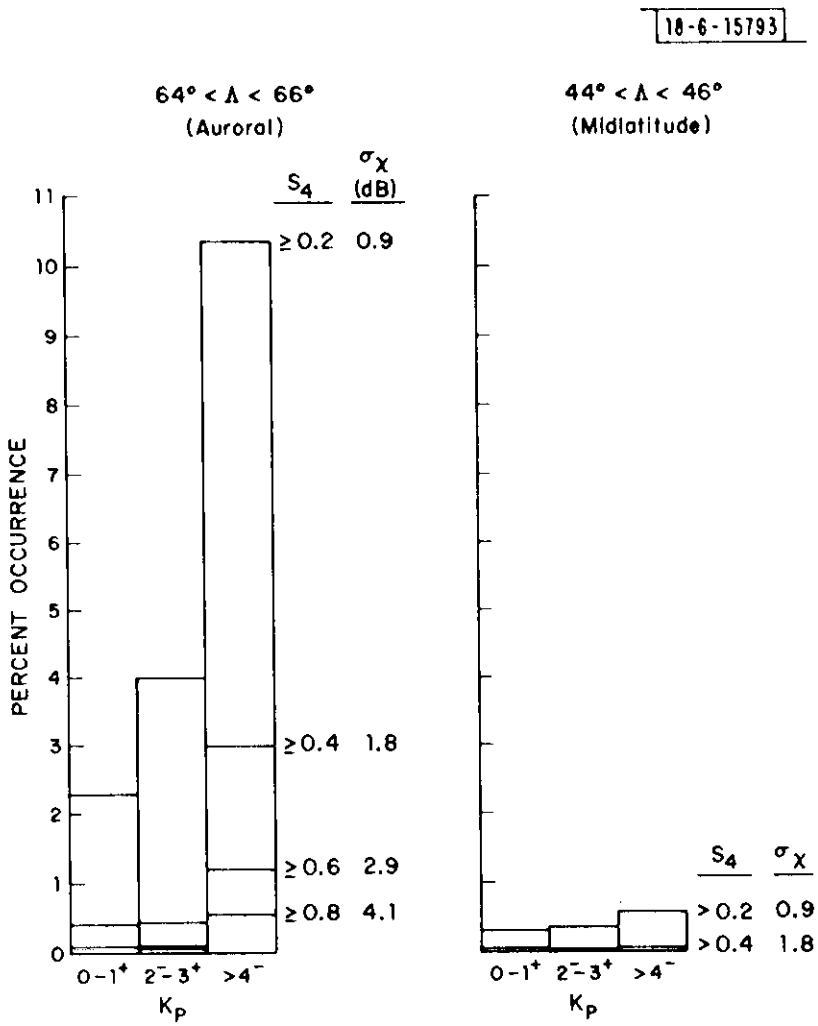

Fig. 31 Magnetic activity dependence of scintillation at 400 MHz for auroral and mid-latitude locations.

time periods with scintillation, the time periods range from one to seven hours.[63] Equatorial scintillation often show patches of scintillation 1/2 to 2 hours long separated by quiet times of the same or shorter duration. Auroral observations show scintillation patches that extend over many degrees of invariant latitude as shown in Fig. 25. These data indicate that scintillation typically occurs in stretches that may last for many minutes. Occasionally single bursts or brief scintillation events are observed in the mid-latitude region.

During a period with scintillation, the signal level fades are relatively rapid. Little data are available on the statistics of fade rate. Koster[65] made crude fade rate estimates for six months of the data obtained during his 1967-1968 observations. He estimated the average fade rate for each five minute interval by counting the number of fades. The results of his analysis show an average fade rate of 6 per minute during the peak evening hours (2200-0200). His data also showed that the average fade rate was correlated with mean scintillation index. For strong scintillation approaching the limit value, an increase in fade rate is expected (see Section II). For weak scintillation more data is required from a number of locations to establish a statistical description of ionospheric irregularity drift velocity as a function of geographical and geophysical parameters.

V. CONCLUSIONS

The auroral region observations clearly show that scintillation will affect system design at frequencies up to at least 400 MHz. The equatorial region observations show that frequencies up to 6 GHz are affected. Since scintillation is clearly a fact of life at UHF and VHF, methods to mitigate its effects are required. While the data are somewhat inadequate, some recommendations can be made. First, some negative recommendations: The two frequency correlation function analyses showed that scintillation is a wideband phenomena and frequency diversity is not practical. The cross polarization observations showed that scintillations on principal and orthogonal circular polarizations were correlated implying that polarization divesity will not work at UHF. While these analyses and measurements were performed for auroral region observations the results also apply in the equatorial region. For the auroral region, the weak scintillation data showed power-law power spectra for electron density irregularities. Preliminary analysis of 254 MHz data reported for the equatorial region[47] also show power law spectra (with a three-dimensional index $p = 4$). This suggests that although the mechanisms causing equatorial region irregularities may be different from those active in the auroral region, the resultant effects of the irregularities on propagation are the same and the results obtained from the Millstone data apply in the equatorial region.

One possible solution is space diversity: The Millstone observations were taken using a low orbiting satellite. The temporal variation of the signal level is caused by the motion of the line-of-sight through the irregularities. The satellite motion is known, hence the temporal variations may be interpreted in terms of the spatial variation of electron density. The frequency scale on Fig. 13 may be interpreted as a wavenumber scale with, for the satellite, receiver geometry pertinent to Fig. 13, the 1-Hz value equivalent to 2π km^{-1} (scale size of 1 km). Since the width of each power spectrum is approximately the reciprocal of the correlation distance, the correlation distance was approximately 0.5 km at UHF and 0.8 km at VHF. This implies that the scintillation observed via rays separated by more than a Fresnel zone radius in the disturbed region of the ionosphere should be uncorrelated and could be combined to get diversity. The required ray separation may be obtained by site diversity or by direct and surface reflected rays. For strong scintillation the power spectrum broadened implying that smaller site diversity distances may be useful in that limit.

Another possible solution is time diversity: The fade duration statistics reported above reflect the motion of the line-of-sight through the medium and, for weak scintillation the duration values should be inversely proportional to the translation velocity of the ray at the height of the irregularities. For geostationary satellites, the line-of-sight is fixed and the

irregularities drift by. The fade duration values then should be inversely proportional to the drift rate. Using a 70 m/sec drift rate, the fade duration should be an order of magnitude longer than those shown in Fig. 6. For strong scintillation, the fade durations should be shorter than for weak scintillation as shown in the discussion of Fig. 6. The power spectra shown in Fig. 13 implied a correlation time the order of 0.5 sec at UHF and 0.8 sec at VHF. As with the fade duration values, the correlation time is dependent upon the velocity of the irregularities perpendicular to the line-of-sight. Since the signal becomes uncorrelated in time, time diversity is also possible. For geostationary satellites, correlation time depends both on the Fresnel zone size and the drift velocity of the irregularities. The latter is a random variable that has to be observed at many locations over a long period of time to provide an adequate statistical description. Since the fade rate or correlation time is different for strong scintillation, observations must be made in the weak scintillation regime to define drift velocities.

VI. RECOMMENDATIONS

The only solutions we have recommended are the use of space or time diversity. Some guidelines for their application may be obtained from Millstone and other available data. However, to optimize system design, more information is required. We recommend:

1. Additional available weak scintillation data should be processed to determine the structure of the power spectrum to establish if the power-law form represents all observations.

2. Available weak scintillation data from geostationary satellite observations should be analyzed to determine drift rate statistics.

3. New observations using both low-orbiting and geostationary satellites with several coherently related carrier frequencies widely spread in the UHF and SHF bands at and above the frequencies of interest should be made to provide adequate statistics of amplitude, phase, and drift velocity. The frequencies should be chosen such that weak scintillation is always observed at one of the frequencies.

Acknowledgment

The author acknowledges the help and support of Drs. J. V. Evans and R. H. Wand of the Millstone Hill radar site in making their data available for analysis and of T. M. Turbett for the data processing.

References

1. C. G. Little and A. Maxwell, "Fluctuations in the Intensity of Radio Waves from Galactic Sources," Phil. Mag. 42, 267-278 (1951).

2. H. E. Whitney, J. Aarons, and C. Malik, "A Proposed Index for Measuring Ionospheric Scintillations," Planet. Space Sci. 17, 1069-1073 (1969).

3. J. Aarons, H. E. Whitney, and R. S. Allen, "Global Morphology of Ionospheric Scintillations," Proc. IEEE 59, 159-172 (1971).

4. R. S. Lawrence, J. L. Jespersen, and R. C. Lamb, "Amplitude and Angular Scintillations of the Radio Source Cygnus-A Observed at Boulder, Colorado," J. of Res. NBS 65D, 333-350 (1961).

5. G. S. Kent, "High Frequency Fading of the 108 Mc/s Wave Radiated From an Artificial Earth Satellite as Observed at an Equatorial Station," J. Atmosph. Terr. Phys. 22 255-269 (1961).

6. C. G. Little, G. F. Reid, E. Stiltner, and R. P. Merritt, "An Experimental Investigation of the Scintillation of Radio Stars Observed at Frequencies of 223 and 456 Megacycles per Second from a Location Close to the Auroral Zone," J. Geophys. Res. 67, 1763-1784 (1962).

7. E. J. Fremouw and H. F. Bates, "Worldwide Behavior of Average VHF-UHF Scintillation," Radio Sci. 6 863-869 (1971).

8. J. R. Koster, "Equatorial Scintillation," Planet. Space Sci. 20, 1999-2014 (1972).

9. N. J. Skinner, R. F. Kelleher, J. B. Hacking and C. W. Benson, "Scintillation Fading of Signals in the SHF Band," Nature 232, 19-21 (1971).

10. R. R. Taur, "Ionospheric Scintillation at 4 and 6 GHz," COMSAT Tech. Rev. 3, 145-163 (1973).

11. H. G. Booker, J. A. Ratcliffe, and D. H. Shinn, "Diffraction from an Ionospheric Screen with Application to Ionospheric Problems," Phil. Tran. Roy. Soc. A242, 579-607 (1950).

12. R. P. Mercier, "Diffraction by a Screen Causing Large Random Phase Fluctuations," Proc. Camb. Phil. Soc. 58 382-400 (1962).

13. B. H. Briggs and I. A. Parkin, "On the Variation of Radio Star and Satellite Scintillations with Zenith Angle," J. Atmosph. and Terr. Phys. 25, 339-365 (1963).

References Cont'd

14. J. R. Koster, "Ionospheric Studies Using the Tracking Beacon on the 'Early Bird' Synchronous Satellite," Ann. de Geophys. 22, 103-107 (1966).

15. J. Pomalaza, R. F. Woodman, G. Tisnado, J. Sandoval and A. Guillev, "A Progress Report on Scintillation Observations at Ancon and Jicamarco Observatories," NASA/GSFC X-520-70-398 NASA Goddard Space Flight Center, Greenbelt, Md. (October 1970).

16. J. Pomalaza, R. F. Woodman, J. Tisnado, and E. Nakasone, "Study of Equatorial Scintillations, A Progress Report," NASA/GSFC X-750-73-244, NASA Goddard Space Flight Center, Greenbelt, Md. (December 1972).

17. K. G. Budden, "The Amplitude Fluctuations of the Radio Wave Scattered from a Thick Ionospheric Layer with Weak Irregularities," J. Atmosph. and Terr. Phys. 27 155-172 (1965).

18. V. I. Tatarskii, The Effects of the Turbulent Atmosphere on Wave Propagation, Nauka, Moscow, 1967; Trans. avail. U. S. Dept. of Comm. National Technical Information Service, Springfield, Va.

19. J. C. Ghiloni, Ed. "Millstone Hill Radar Propagation Study: Instrumentation," Technical Report 507, Lincoln Laboratory, M.I.T. (20 September 1973), DDC AD-775140.

20. G. R. Ochs and R. S. Lawrence, "Saturation of Laser-Beam Scintillation Under Conditions of Strong Atmospheric Turbulence," J. Optical Soc. Amer. 59 226-227 (1969).

21. J. R. Dunphy and J. R. Kerr, "Scintillation Measurements for Large Integrated-Path Turbulence," J. Optical Soc. Amer. 63, 981-986 (1973).

22. K. Bischoff and B. Chytil, "A Note on Scintillation Indices," Planet. Space Sci. 17, 1059-1066 (1969).

23. C. L. Rino and R. J. Fremouw, "Statistics for Ionospherically Diffracted UHF/VHF Signals," Radio Sci. 7, 1095-1104 (1972).

24. H. E. Whitney, J. Aarons, R. S. Allen and D. R. Seemann, "Estimation of the Cumulative Amplitude Probability Distribution Function of Ionospheric Scintillation," Radio Sci. 7, 1095-1104 (1972).

25. M. Nakagami, "The m-distribution--A General Formula of Intensity Distribution of Rapid Fading," in Statistical Methods on Radio Wave Propagation, ed. W. C. Hoffman, (Pergamon Press, New York, 1960).

References Cont'd

26. C. L. Rufenach, Power-Law Wavenumber Spectrum Deduced from Ionospheric Scintillation Observations," J. Geophys. Res. 77, 4761-4772 (1972).

27. D. G. Singleton, "Power Spectra of Ionospheric Scintillations," J. Atmosph. and Terr. Phys. 36, 113-133 (1974).

28. T. J. Elkins and M. D. Papagiannis, "Measurement and Interpretation of Power Spectrums of Ionospheric Scintillation at a Subauroral Location," J. Geophys. Res. 74, 4105-4115 (1969).

29. O. K. Garriott, A. V. daRosa, "Electron Content Obtained from Faraday Rotation with Phase Length Variations," J. Atmosph. and Terr. Phys. 32, 705-727 (1970)

30. L. J. Porcello and L. R. Hughes, "Observed Fine Structure of a Phase Perturbation Induced During Transauroral Propagation,: J. Geophys. Res. 73, 6337-6346 (1968).

31. H. E. Whitney and W. F. Ring, "Dependency of Scintillation Fading of Oppositely Polarized VHF Signals," IEEE Trans. Antennas and Propagat. AP-19, (1971).

32. J. R. Koster, "Ionospheric Studies Using the Tracking Beacon on the 'Early Bird' Synchronous Satellite," Ann. de Geophys. 22, 435-439 (1966).

33. H. A. Blank and T. S. Golden, "Analysis of VHF/UHF Frequency Dependence, Space, and Polarization Properties of Ionospheric Scintillation in the Equatorial Region," 1973 IEEE Inter. Comm. Conf. Proc. 17-27 to 17-35, (June 1973).

34. J. P. McClure, "Polarization Measurements During Scintillation of Radio Signals from Satellites," J. Atmosph. and Terr. Phys. 27, 335-348 (1965).

35. R. S. Roger, "The Effect of Scintillations on the Polarization of Satellite Transmissions near 20 Mc/s," J. Atmosph. and Terr. Phys. 27, 335-348 (1965).

36. P. L. Dyson, J. P. McClure, and W. B. Hanson, "In-Situ Measurements of the Spectral Characteristics of F Region Ionospheric Irregularities," J. Geophys. Res. 79 1497-1502 (1974)

37. A. T. Young, "Interpretation of Interplanetary Scintillations," Astrophys. J. 168, 543-562 (1971).

References Cont'd

38. S. Basu, R. S. Allen, and J. Aarons, "A Detailed Study of a Brief Period of Radio Star and Satellite Scintillations," J. Atmosph. and Terr. Phys. 26, 811-823 (1964).

39. J. Aarons, "Ionospheric Irregularities at Arecibo, Puerto Rico," J. Atmosph. and Terr. Phys. 29, 1619-1624 (1967).

40. H. J. A. Chivers, "The Simultaneous Observation of Radio Star Scintillations on Different Radio-Frequencies," J. Atmosph. and Terr. Phys. 17, 181-187 (1960).

41. H. J. A. Chivers and R. D. Davies, "A Comparison of Radio Star Scintillation at 1390 and 79 Mc/s at Low Angles of Elevation," J. Atmosph. and Terr. Phys. 24 573-584 (1962).

42. J. Aarons, R. S. Allen, and T. J. Elkins, "Frequency Dependence of Radio Star Scintillations," J. Geophys. Res. 72, 2891-2902 (1967).

43. R. S. Allen, "Comparison of Scintillation Depths of Radio Star and Satellite Scintillations," J. Atmosph. and Terr. Phys. 31 289-297 (1969).

44. H. D. Craft, Jr. and L. H. Westerlund, "Scintillation at 4 and 6 GHz Caused by the Ionosphere," AIAA 10th Aerospace Sciences Meeting, San Diego, Calif., January 1972.

45. J. M. Lansinger and E. J. Fremouw, "The Scale Size of Scintillation Producing Irregularities in the Auroral Ionosphere," J. Atmosph. and Terr. Phys. 29, 1229-1242 (1967).

46. K. Burrows and C. G. Little, "Simultaneous Observations of Radio Star Scintillations on Two Widely Spaced Frequencies," Jodrell Bank Ann. 1, 29-35 (1952).

47. M. R. Paulson and R. V. F. Hopkins, "Effects of Equatorial Scintillation Fading on Satcom Signals," NELC/TR 1875, Naval Electronics Laboratory Center, San Diego, Calif. (May 1973).

48. R. R. Taur, Private Communications (1973).

49. K. G. Budden, "The Theory of the Correlation of Amplitude Fluctuations of Radio Signals at Two Frequencies Simultaneously Scattered by the Ionosphere," J. Atmosph. and Terr. Phys. 27, 228-297 (1965).

50. C. E. McIlwain, "Coordinates for Mapping the Distribution of Magnetically Trapped Particles," J. Geophys. Res. 66, 3681-3691 (1961).

References Cont'd

51. H. E. Whitney, Private Communication (1974).

52. S. F. Clifford, G. R. Ochs, and R. S. Lawrence, "Saturation of Optical Scintillation by Strong Turbulence," J. Optical Soc. Amer. 64, 148-154 (1974).

53. T. J. Elkins, "Summary of Properties of F-Region Irregularities," In "A Survey of Scintillation Data and its Relationship to Satellite Communications," AGARD Rept. 571, 13-37, (August 1969).

54. J. R. Koster and I. K. Katsriku, "Some Equatorial Ionospheric E- and F-Region Drift Measurements at Tamale," Ann. de Geophys. 22, 440-447 (1966).

55. J. R. Koster and R. W. Wright, "Scintillation, Spread-F, and Trans-equatorial Scatter," J. Geophys. Res. 65, 2303-2306 (1960).

56. C. Huang, "F-Region Irregularities that Cause Scintillation and Spread-F at Low Latitude," J. Geophys. Res. 75, 4833-4841 (1970).

57. M. Dagg, "Radio-Star Ridges," J. Atmosph. and Terr. Phys. 11, 118-127 (1957).

58. M. Anastassiades, D. Matsoukas, and G. Moritis, "40 MHz Ionospheric Scintillation and the Sporadic E Layer," Radio Sci. 5, 953-957 (1970).

59. A. A. Chen, P. N. Chin, and M. P. Chance, "Field Line Connection Between Scintillation and Ionospheric Conditions Causing Spread-E," J. Geophys. Res. 77, 1859-1868 (1972).

60. D. H. Clark, J. Mawdsley and W. Ireland, "Mid-Latitude Radio Star Scintillation: The Height of the Irregularities," Planet. Space Sci. 18, 1785-1791 (1970).

61. Joint Satellite Studies Group, "On the Latitude Variation of Scintillations of Ionospheric Origin in Satellite Signals," Planet. Space Sci. 16, 775-781 (1968).

62. J. V. Evans, Ed., "Millstone Radar Propagation Study: Scientific Results," Technical Report 509, Lincoln Laboratory, M.I.T. (13 November 1973).

63. B. E. Nichols, "UHF Fading from a Synchronous Satellite Observed at Kwajalein October 1970 Through June 1972," Technical Note 1974-19, Lincoln Laboratory, M.I.T. (22 March 1974).

References Cont'd

64. J. P. Mullen and H. E. Whitney, "Equatorial Measurements Using the LES-6 and ATS-3 Satellite Beacons," AFCRL (1973).

65. J. R. Koster, "Equatorial Studies of the VHF Signal Radiated by Intelsat III, F-3: 1. Ionospheric Scintillation," Prog. Rept. 3, Dept. of Physics, Univ. of Ghana, September 1968 (AD 681462).

66. E. Nielson and J. Aarons, "Satellite Scintillation Observations Over the Northern High Latitude Regions," J. Atmosph. and Terr. Phys. 36, 159-165 (1974).

67. J. A. Aarons, J. Mullan, and S. Basu, "The Statistics of Satellite Scintillation of a Subauroral Latitude," J. Geophys. Res. 69, 1785-1794 (1964).

68. J. L. Jesperson and J. Kamas, "Satellite Scintillation Observations at Boulder, Colorado," J. Atmosph. and Terr. Phys. 26 457-473 (1964).

69. J. Sinclair and R. F. Kelleher, "The F-Region Equatorial Irregularity Belt as Observed from Scintillation of Satellite Transmission," J. Atmosph. and Terr. Phys. 31 201-206 (1969).

70. P. R. Kranz and K. C. Yeh, "Scintillation Observations of Satellite Signals," J. Atmosph. and Terr. Phys. 27, 1169-1176 (1964).

71. J. Aarons, "A Descriptive Model of F-Layer High Latitude Irregularities as Shown by Scintillation Observations," J. Geophs. Res. 78 7441-7450 (1973).

72. R. M. Davis, Jr., "The Occurrence of Spread-F and Its Effects on HF Propagation," Rept. OT/TRER 28 Institute for Telecommunication Sciences, Boulder, Colorado (March 1972).

OUTSIDE DISTRIBUTION LIST

Dr. Joseph de Bettencourt
Raytheon Company
Equipment Division Hdqts.
430 Boston Post Road
Wayland, Mass. 01778

Mr. James H. Kluck
Aerospace Corporation
Communications Section
P. O. Box 1308
San Bernardino, Calif. 92401

Mr. John M. Goodman, Code 5370G
Naval Research Laboratory
Washington, D. C. 20390

Mr. Robert L. Feik, Director
Operations Research Analysis
AFCS (CSMOA)
Scott AFB, Illinois

Prof. Ferrel G. Stremler
Dr. W. P. Birkemeier
The University of Wisconsin
Dept. of Electrical Eng.
Madison, Wisconsin 53706

Mr. John Alishouse
National Environmental Satellite Cen.
NOAA
Washingtion, D. C. 20233

Capt. John F. Kauntak, SREE
Directorate of Eng. Sciences
AF Office of Scientific Res. (OAR)
Arlington, Virginia 22209

Mr. John J. Kelleher
National Scientific Laboratories
Westgate Research Park
McLean, Virginia 22101

Dr. Paul J. Titterton
Sylvania Electronics System
P. O. Box 188, Ellis St. Bldg.
Mountain View, CA. 94040

Dr. John Lane
Radio and Space Research Station
Ditton Park, Slough, Bucks
ENGLAND

Dr. Aldo Paraboni
Instituto de Electtrotechina ed
Electtronica
Via Ponzio 34/5
20133 Milano
ITALY

Dr. H. S. Hayre
Cullen College of Engineering
University of Houston
Cullen Blvd.
Houston, Texas 77004

Mr. Robert A. Begun
E. Bollay Assoc., Inc.
P. O. Box 1022
Boulder, Colorado 80302

Engineering Library
Collins Radio Company
Dallas, Texas

Mr. James R. Poppe
General Electric Company
Mountain View Plant
Lynchburg, Virginia

Dr. Wolfgang Kummer
Dr. A. D. Whellon
Mr. V. F. Cashen

Hughes Aircraft Company
Aerospace Group
Culver City, Calif.

Mr. R. E. Alexovich, Code 9701
Mr. Perry W. Kuhns, Code 24611

NASA
Louis Research Center
2100 Brookpark Road
Cleveland, Ohio 44135

Mr. H. M. Lawrence, Stop 490
Langley Research Center
NASA
Langley Station, Virginia

Mr. V. F. Henry, Code 733
Mr. Frank X. Downey
Dr. Jerome Eckerman Code 750
Mr. Louis Ippolito
Mr. William Binkley

NASA
Goddard Space Flight Center
Greenbelt, Maryland 20771

Mr. Jeff Bonelle
TRW Systems Group
1 Space Park
Redondo Beach, CA. 90278

Mr. E. C. Hamilton, Code R-ASTR-A
Mr. T. A. Barr, Code R-ASTR-A
NASA
Marshall Space Flight Center
Alabama 35812

Dr. Richard Marsten Code EC
Mr. Greg Andrus Code EC
Mr. J. B. McElroy, Code TN
Mr. J. Freibaum, ECF (5)

NASA Headquarters
Washington, D. C. 20546

Dr. Earl Gossard
Dr. Gordon Little
Mr. Martin Decker
Wave Propagation Laboratory
NOAA
Boulder, Colorado 80302

Dr. D. Wortendyke
Mr. R. Hubbard
Mr. C. B. Emmanuel
Mr. W. E. Johnson
Mr. P. Wells
Mr. Albrecht P. Barsis
Mr. Evan J. Dutton

Department of Commerce
Office of Telecommunications
ESSA Research Laboratories
Boulder, Colorado 80302

Dr. Edwin Kessler
Dr. Richard J. Doviak

National Severe Storm Laboratory
Norman, Oklahoma

Mr. Walter E. Buehler
The Boeing Company
Stop 16-28
Seattle, Washington

Mr. A. H. LaGrone
University of Texas
Eng. Science Bldg. 535
Austin, Texas 78712

Mr. John Bottomley
Northrop Page Comm. Eng.
3300 Whitehaven St., N. W.
Washington, D. C. 20507

Mr. J. L. Levatich
COMSAT Laboratories
1835 K Street, N. W.
Washington, D. C. 20006

Prof. A. T. Waterman, Jr.
Stanford Electronics Laboratories
Stanford, Calif. 94305

Mr. N. R. Ortwein, Code S250.1
Naval Electronics Lab Center
San Diego, Calif. 92152

Mr. Glen H. Kertel
San Hose State College
Dept. of Electrical Engineering
San Jose, Calif. 95114

Mr. J. F. Roche
Raytheon Company
1415 Boston Providence Highway
Norwood, Mass.

Prof. R. Bolgiano, Jr.
Cornell University
Phillips Hall
Ithaca, New York 14850

Mr. L. Maynard
Dr. Bertram Bleves
Dr. J. I. Strickland
Mr. J. W. B. Day
Dr. K. S. McCormick

Communications Research Center
P. O. Box 490, Terminal A
Ottawa, Ontario CANADA KIN8T5

Mr. Richard Gould
Mr. Roger Carey
Mr. Harry Fine

FCC
1919 M St., N. W.
Washington, D. C. 20554

Dr. D. B. Large
Westinghouse Electric Corp.
Georesearch Laboratory
8401 Baseline Road
Boulder, Colorado 80302

Dr. John Dubzinsky
The Rand Corporation
1700 Main Street
Santa Monica, CA 90406

Dr. M. J. Voge
Direction du C. N. E. T.
3, Avenue de la Republique
Issey-les-Monlineau (Seine)
FRANCE

Dr. John P. Hagen
Penn State University
102 Whitmore Laboratory
University Park
Pennsylvania 16802

Mr. L. A. Gausman
American Tel. and Tel. Co.
Room 904
1 North Wacker Drive
Chicago, Illinois 60606

Prof. Olof Rydbeck, Director
Research Lab. of Electronics
Chalmers University of Technology
Gothenburg, SWEDEN

Dr. A. N. Ince, Chief
Communications Division
SHAPE Technical Center
The Hague, HOLLAND

Mr. F. Gall
ACRES Intertel, Ltd.
298 Elgin Street
Ottawa 4, CANADA

Mr. P. A. Bergin, Mail Zone 580-10
General Dynamics
P. O. Box 1128
San Diego, Calif. 92112

Dr. James R. Wait (Rm. 231 Bldg 1)
Dr. Clifford Rufenach
Joseph Pope
Richard Grubb

NOAA-Environmental Research Lab
Boulder, Colo. 80302

Prof. James Massey
Dept. of Electrical Engineering
University of Notre Dame
Notre Dame, Indiana 46556

Mr. Robert Hopkins
Code 2420
US Naval Electronics Lab Center
San Diego, Calif. 92152

Don Jansky
Office of Telecommunications Policy
1800 G. Street, NW
Washington, DC 20504

Richard Kirby
Institute for Telecommunication Sci.
Boulder, Colo 80302

Wilford E. Brown
Transportation Systems Center
55 Broadway
Cambridge, MA 02139

Dr. Charles N. Rino
Stanford Research Institute
Menlo Park, Calif. 94025

Dr. Fred Rhode
Engineer's Topographic Lab
Us Army
Ft. Belvoir, Va.

Mr. John Martin
Code 863
Goddard Space Flight Center
Greenbelt, Md. 20771

Mr. Barry Mendoza
Philco-Ford
Mail Stop G-80
3939 Fabian Way
Palo Alto, Calif. 94303

Dr. J. P. McClure
University of Texas
Box 30365
Dallas, Texas 75203

Mr. Keith D. McDonald
DNSS Planning Group
801 N. Randolph Street
Arlington, Va. 22203

Dr. Robert W. Rochelle
Code 750
Goddard Space Flight Center
Greenbelt, Md. 20771

Dr. Hiam Soicher
AMSEL-TR-AI
US Army Electronics Command
Ft. Monmouth, NJ 07703

William Utlaut
Dept. of Commerce (OT/ITS)
Boulder, Colo. 80302

Prof. K. C. Yeh
Dept. of Electrical Engineering
University of Illinois
Urbana, IL 61801

Dr. Roger Taur
COMSAT Laboratories
Clarksburg, Maryland 20734

Cmdr. Roger Berg
Navy Communications Headquarters
N77B
4401 Massachusetts Avenue, N. W.
Washington, DC 20390

Prof. Rodger E. Ziemer
123 Electrical Engineering Bldg.
University of Missouri-Rolla
Rolla, Missouri 65401

Vernon E. Hilderbrand
Code 2200
NEL/NWC
San Diego, CA 92152

Mr. Walter Melton
Aerospace Corporation
P. O. Box 95803
Los Angeles, CA 90045

The Defense Documentation Center
ATTN: TISIA-1 (2)
Cameron Station, Bldg. 5
Alexandria, Virginia 22314

Commander
Naval Electronic Systems Command
(PME-106-4)
Dept. of the Navy
Washington, DC 20360 (4)

Chief of Naval Operations (OP 941E)
Department of the Navy
Washington, DC 20350

Defense Communications Agency
8th and South Courthouse Road
Arlington, Virginia 22204
Attn: Dr. Frederick Bond

Commander
Naval Electronics Lab Center-Library
San Diego, Calif. 92152

U.S. Naval Research Laboratory
Code 5405
Washington, D.C. 20390
Attn: Lt. Cdr. N. L. Wardle

U.S. Navy Underwater Systems Center
New London Laboratory
Ft. Trumbull
New London, Connecticut 06321
Attn: Mr. John Merrill

Mr. K. Bullington
Mr. L. T. Gusler
Mr. R. W. Wilson
Dr. D. C. Hogg
Mr. James M. Kelly

Bell Telephone Laboratories
Crawford Corner Road
Holmdel, New Jersey 07733

Naval Postgraduate School
Electrical Engineering Dept.
Montere, Calif. 93940
Attn: Prof. John Ohlson, Code 52

Commander
Naval Electronics System Command
(PME-117)
Dept. of the Navy
Washington, DC 20360

G. E. LaVean
Defense Communications Eng. Center
Reston, Virginia

Mr. I. Katz
Vincent L. Piscane
Michael M. Feen

The Johns Hopkins University
Applied Physics Lab
8621 Georgia Avenue
Silver Springs, Md.

Mr. Herbert Whitney
Dr. Jules Aarons

AFCRL (LIR)
L. G. Hanscom Field
Bedford, Ma. 01730

Mr. C. C. Ingram
Dr. Howard Blank

Computer Sciences Corp.
6565 Arlington Blvd.
Falls Church, VA. 22046

Charles Brooks, ARD 250
Federal Aviation Administration
800 Independence Avenue, S. W.
Washington DC 20591

Ronald Beard
Rudolph Zirm

Code 7969
Naval Research Lab
Washington, DC 20375

Dow Evelyn
Headquarters DNA
Washington, DC 20305

Roy E. Anderson
General Electric Company
Research and Development Center
Schnectady, New York

Dr. W. S. Ament
Code 5404
Naval Research Lab
Washington, DC 20375

Harry Feigleson, Code M930
Maritime Administration
Dept. of Commerce
14th and E Streets, N. W.
Washington, DC 20234

Dr. Edward J. Fremouw
Stanford Research Institute
Menlo Park, Calif. 94025

Thomas S. Golden Code 751
Robert Godfrey Code 831
Goddard Space Flight Center
Greenbelt, Md. 20771

George Haroules
Transportation Systems Center
55 Broadway
Cambridge, Ma. 02139

Mr. Edward Wolff
John E. Jackson
Code 750.1
Goddard Space Flight Center
Greenbelt, Md. 20771

Allen Johnson
USAT-Avionics Lab
AFAL/AAI
WPAFB, Ohio

Mr. Fumio Minozuma
Hitachi, Ltd.
NIPPON Bldg.
No. 6-2, 2-chome, Oktemachi
Chiyoda-ku, Tokyo 100 JAPAN

Dr. P. Ramakrishna Rao
Elec. Engineering Dept.
Indian Institute of Technology
Kanput-16
INDIA

Ronald Woodman, Director
Radio Observatorio de Jicamarca
Instituto Geofisico Del Peru
Apartado 2747
Lima, PERU

Dr. Bello
CNR
381 Elliot Street
Newton, MA. 02164

Mr. J. Potts
Mr. Hans Weiss
COMSAT Corporation
1900 L St., N.W.
Washington, D.C. 20036

Dr. Edward C. Reifenstein, III
Dr. Norman E. Gaut

Environmental Research and Tech., Inc.
429 Manett Road
Lexington, Mass.

Dr. Colin D. Watkins
Royal Radar Establishment
Leigh Sinton Road
Malvern, Worcestershire,
ENGLAND

Dr. Bradford Bean
Environmental Research Lab
NOAA
Boulder, Colorado 80302

Mr. Paul D. Newhouse
Electromagnetic Compatibility
Analysis Center
USN Marine Eng. Lab
Annapolis, Maryland 21402

Mr. D. E. Sakhia, Code MP-71
Martin Company
Orlando, Florida 32805

Prof. Walton W. Cannon
Virginia Polytechnic Institute
Virginia Assoc. Research Center
12070 Jefferson Avenue
Newport News, Virginia 23606

Mr. John F. Fowler
Lockheed Missiles and Space Co.
Lockheed Aircraft Corp.
Sunnyvale, Calif.

Mr. M. W. Hotowitz
Sanders Associates, Inc.
6621 Electronics Drive
Springfield, Virginia 22151

Mr. Wilfred Dean
Office of Telecommunications Policy
1800 G St., N. W.
Washington, D. C. 20504

Dr. E. Schanda
Institut fur Augewandte Physik
Bern, Sidlerstrasse 5
SWITZERLAND

Mr. R. B. Beam
Area Manager-Planning
General Telephone and Electronics International
730 Third Avenue
New York, N. Y. 10012

Mr. David Davidson
Mr. Charles B. Frye
Sylvania Electronics System
Applied Research Laboratory
40 Sylvan Road
Waltham, Mass. 02154

Prof. Ivo Rauzi
Instituto Sup. P. T.
Viale Trastevere, 189
00153, Rome ITALY

N. J. Zabusky
Bell Telephone Labs
Whippany, N. J. 07981

Mr. L. M. Guyot
Liznes Telegraphiques and Telephonique
78 Conflaus Sainte Honorine
FRANCE

Mr. J. H. Best (Alt. for Dr. Johnson
US Army SAFEGUARD System Office
Commonwealth Building
1320 Wilson Boulevard
Arlington, Virginia 22209

Dr. R. S. Ruffine (Chairman)
US Army Advanced Ballistic Missile Defense Agency
Commonwealth Bldg.
1320 Wilson Blvd.
Arlington, VA 22209

Mr. J. H. W. Unger
Room 1K-233
Bell Telephone Laboratories, Inc.
Whippany Road
Whippany, New Jersey 07981

Dr. L. J. Fretwell
Room 1K-206
Bell Telephone Laboratories, Inc.
Whippany Road
Whippany, New Jersey 07981

Dr. R. W. Hendrick
Mission Research Company
812 Anacapa Street
Santa Barbara, CA 93102

Mr. R. L. Leadabrand
Stanfrod Research Institute
Radio Physics Laboratory
Menlo Park, CA. 94025

Dr. G. H. Millman
General Electric Company
HMED, Court Street Plant
Syracuse, New York 13201

Russell Brown
Mr. Vignetti
Robert LaFondra

Naval Research Laboratory
Washington, DC 20390

Mr. H. A. Perry
Naval Ordinance Laboratory
New Hampshire Avenue
Silver Springs, MD 20910

S. G. Reed, Jr.
Assistant Chief Scientist
Dept. of the Navy
Office of Naval Research
ONR:102T:SGR:av
Arlington, VA. 22217

UNCLASSIFIED

SECURITY CLASSIFICATION OF THIS PAGE *(When Data Entered)*

REPORT DOCUMENTATION PAGE		READ INSTRUCTIONS BEFORE COMPLETING FORM
1. REPORT NUMBER ESD-TR-74-212	2. GOVT ACCESSION NO.	3. RECIPIENT'S CATALOG NUMBER
4. TITLE *(and Subtitle)* Morphology of Ionospheric Scintillation		5. TYPE OF REPORT & PERIOD COVERED Technical Note 6. PERFORMING ORG. REPORT NUMBER Technical Note 1974-29
7. AUTHOR*(s)* Crane, Robert K.		8. CONTRACT OR GRANT NUMBER*(s)* F19628-73-C-0002
9. PERFORMING ORGANIZATION NAME AND ADDRESS Lincoln Laboratory, M.I.T. P.O. Box 73 Lexington, MA 02173		10. PROGRAM ELEMENT, PROJECT, TASK AREA & WORK UNIT NUMBERS Project No. 1508A
11. CONTROLLING OFFICE NAME AND ADDRESS Naval Electronic Systems Command Department of the Navy Washington, DC 20360		12. REPORT DATE 21 May 1974 13. NUMBER OF PAGES 98
14. MONITORING AGENCY NAME & ADDRESS *(if different from Controlling Office)* Electronic Systems Division L.G. Hanscom Field Bedford, MA 01730		15. SECURITY CLASS. *(of this report)* Unclassified 15a. DECLASSIFICATION DOWNGRADING SCHEDULE

16. DISTRIBUTION STATEMENT *(of this Report)*

Approved for public release; distribution unlimited.

17. DISTRIBUTION STATEMENT *(of the abstract entered in Block 20, if different from Report)*

18. SUPPLEMENTARY NOTES

None

19. KEY WORDS *(Continue on reverse side if necessary and identify by block number)*

communication systems
Millstone Hill radar
ionospheric scintillation

20. ABSTRACT *(Continue on reverse side if necessary and identify by block number)*

This report is directed toward providing information to communication systems designers first about scintillation as observed in a single experiment, second about the adequacy of the existing models used to interpret scintillation data, and finally about the variation of scintillation with geophysical parameters.

DD FORM 1 JAN 73 1473 EDITION OF 1 NOV 65 IS OBSOLETE

UNCLASSIFIED

SECURITY CLASSIFICATION OF THIS PAGE *(When Data Entered)*